ABSTRACT

Title of Document: INVESTIGATION INTO THE POTENTIAL TOXICITY OF ZERO-VALENT IRON NANOPARTICLES TO A TRICHLOROETHYLENE-DEGRADING GROUNDWATER MICROBIAL COMMUNITY

Kara M. Zabetakis, Master of Science, 2013

Directed By: Professor Alba Torrents, Department of Civil and Environmental Engineering

The microbiological impact of zero-valent iron remediation of groundwater was investigated by exposing a trichloroethylene-degrading anaerobic microbial community to bare and coated iron nanoparticles. Changes in population numbers and metabolic activity were analyzed using qPCR and were compared to those of a blank, negative, and positive control to assess for microbial toxicity. Additionally, these results were compared to those of samples exposed to an equal concentration of iron filings in an attempt to discern the source of toxicity. Statistical analysis revealed that the three iron treatments were equally toxic to total Bacteria and Archaea populations, as compared with the controls. Therefore, toxicity appears to result either from the release of iron ions and the generation of reactive oxygen species, or from alteration of the redox system and the disruption of microbial metabolisms. There does not appear to be a unique nanoparticle-based toxicity.

INVESTIGATION INTO THE POTENTIAL TOXICITY OF ZERO-VALENT IRON NANOPARTICLES TO A TRICHLOROETHYLENE-DEGRADING GROUNDWATER MICROBIAL COMMUNITY

By

Kara M. Zabetakis

Thesis submitted to the Faculty of the Graduate School of the
University of Maryland, College Park, in partial fulfillment
of the requirements for the degree of
Master of Science
2013

Advisory Committee:
Professor Alba Torrents, Chair
Professor Sheryl H. Ehrman
Assistant Professor Stephanie A. Yarwood

Acknowledgements

I would like to express my appreciation for the unending support of my advisor, Dr. Alba Torrents. Without her constant aid and mentorship, this thesis would not have been possible. I would also like to thank my committee members: Dr. Sheryl Ehrman, for her insights into experimental design and nanoparticle characterization, and Dr. Stephanie Yarwood, for teaching essential molecular biology techniques and assisting with problems that arose during experimentation.

I am also grateful for the aid of Laura McConnell, Cathleen Hapeman, and Pat Millner of the U. S. Department of Agriculture, Agricultural Research Service (USDA-ARS). Their contributions, along with those of fellow graduate students Gabriela Niño de Guzmán and Daniel Michaelson, were essential for the preliminary stages of design and experimentation.

Finally, I acknowledge the support of the Maryland Surface Analysis Center and the Maryland NanoCenter and its NispLab. The Surface Analysis Center and NispLab are supported in part by the NSF as MRSEC Shared Experimental Facilities.

Table of Contents

Acknowledgements ii

Table of Contents iii

List of Tables v

List of Figures vi

List of Abbreviations vii

Chapter 1: Introduction 1
1.1 Trichloroethylene Contamination and Fate in the Environment 1
1.2 Anaerobic Biodegradation of Trichloroethylene 2
1.3 Engineered Remediation of Trichloroethylene Using Zero-Valent Iron 4
1.4 Potential Toxicity of Zero-Valent Iron Nanoparticles 6
1.5 Research Questions and Experimental Overview 7

Chapter 2: Materials and Methods 9
2.1 Sample Collection 9
2.2 Microcosm Preparation 9
2.3 Enrichment Culture Preparation 10
2.4 Nanoparticle Preparation and Characterization 11
2.4.1 Commercial Supplies 11
2.4.2 Solution Preparation 12
2.4.3 Zeta Potential Determination 13
2.4.4 Transmission Electron Microscopy 14
2.4.5 X-ray Photoelectron Spectroscopy 14
2.5 Toxicity Study 15
2.5.1 Enrichment Culture Spiking 15
2.5.2 Solution Sampling 15
2.5.3 RNA Extraction 16
2.5.4 cDNA Strand Synthesis 18
2.6 Quantitative Polymerase Chain Reaction Analysis 19
2.6.1 Preparation of Standards 19
2.6.2 Verification Reactions 21
2.6.3 Protocol Optimization 23
2.6.4 Test for Inhibition 25
2.6.5 Analysis of Experimental Samples 27
2.7 Statistical Analysis 29

Chapter 3: Results 31
3.1 Nanoparticle Characterization 31
3.1.1 Zeta Potential 31
3.1.2 Transmission Electron Microscopy 32
3.1.3 X-ray Photoelectron Spectroscopy 36
3.2 Water Chemistry 38
3.2.1 pH 38
3.2.2 Oxidation-Reduction Potential 39
3.3 Microbial Enumeration 41
3.4 Analysis of Variance 46

Chapter 4: Discussion 49
4.1 Comparison of Nanoparticle Properties 49
4.2 Relationship between Water Chemistry and Microbial Ecology 51
4.3 Impact of Experimental Treatment 53

Chapter 5: Conclusion 56
5.1 Significance 56
5.2 Future Work 57

Appendices 58
Appendix A: Experimental Diagram 58
Appendix B: Gene Copy Number Calculation 59
Appendix C: Optimum qPCR Conditions 59
Appendix D: XPS Surveys 59
Appendix E: XPS Depth Profiles 65
Appendix F: Sample Concentration Calculation 69
Appendix G: Welch ANOVA Results 69

References 75

List of Tables

		Page
Table 2.1	Primer sets for the qPCR assays	22
Table 3.1	Zetasizer measurements of zeta potential, electrophoretic mobility, and conductivity for the nanoparticle solutions	31
Table 3.2	High-resolution XPS data from particle surveys and element specific analyses for the Ag and Fe nanoparticles	36

List of Figures

		Page
Figure 1.1	Reductive dechlorination of TCE and its daughter species	2
Figure 1.2	Chemical processes involved in dehalorespiration	3
Figure 3.1	Low and high resolution TEM images of the silver nanoparticles	33
Figure 3.2	Low and high resolution TEM images of the bare nanoparticles	34
Figure 3.3	Low and high resolution TEM images of the coated nanoparticles	35
Figure 3.4	Sample pH vs. exposure time for the six experimental treatments	38
Figure 3.5	Sample ORP vs. exposure time for the six experimental treatments	40
Figure 3.6	Eubacteria 16S rRNA gene copies/mL culture vs. time for the six experimental treatments	42
Figure 3.7	Archaea 16S rRNA gene copies/mL culture vs. time for the six experimental treatments	44
Figure 3.8	Dissimilatory sulfate reductase gene copies/mL culture vs. time for the six experimental treatments	45

List of Abbreviations

TCE	Trichloroethylene
cis-DCE	cis-Dichloroethene
VC	Vinyl chloride
ZVI	Zero-valent iron
bulk Fe	Macro-scale iron filings
nZVI	ZVI nanoparticles
bare nZVI	nZVI without any surface modifiers
coated nZVI	nZVI with an inorganic and/or organic surface modifier
tceA	Trichloroethene reductive dehalogenase
vcrA	VC reductase
ORP	Oxidation-reductase potential
qPCR	Quantitative polymerase chain reaction
PVP-Ag NPs	Silver nanoparticles with a polyvinylpyrrolidone surface coating
TEM	Transmission electron microscopy
XPS	X-ray photoelectron spectroscopy
RT-	Reverse transcriptase negative
LB	Lysogeny broth
Eub	Eubacteria
Arc	Archaea
dsr	Dissimilatory sulfate reductase
mcr	Methyl coenzyme M reductase
Dhc	*Dehalococcoides* spp.
Ct	Threshold cycle
BSA	Bovine serum albumin
GCN	Gene copy number
SSA	Specific surface area
E_h	Reduction potential

Chapter 1: Introduction

1.1 Trichloroethylene Contamination and Fate in the Environment

Trichloroethylene (TCE) is a hazardous environmental contaminant due to its widespread use in industry, tendency for long-range transport, resistance to natural attenuation, and potential for adverse toxicological effects.[1-6] Many environmental regulations target the release of this chemical, but introduction into the environment is a continued ecological problem because of its extensive use as an industrial solvent and degreasing agent.[7-9] TCE is often found as a groundwater contaminant after being released into the environment, because it has a tendency to form dense, non-aqueous phase liquids.[2-5] According to the Agency for Toxic Substance and Disease Registry (ATSDR), the extent of this pollution is widespread. The ATSDR estimates that TCE can be found in between 9 and 34 percent of all U.S drinking wells, with many sites above the legal drinking limit.[8] TCE is also listed as the most common groundwater contaminant in U.S. superfund sites, with at least 861 locations targeted for long-term cleanup.[8,9] TCE contamination can cause extensive adverse health effects in humans and aquatic life.[8-11] The contaminant is a suspected carcinogen and a known central nervous system depressant; it can also cause liver and kidney damage with high levels of exposure.[10,11]

TCE can be degraded via step-wise dechlorination to *cis*-dichloroethene (*cis*-DCE), vinyl chloride (VC), and eventually ethene.[12,13] The schematic diagram below depicts this chemical process, which is typically favorable in most reducing systems.

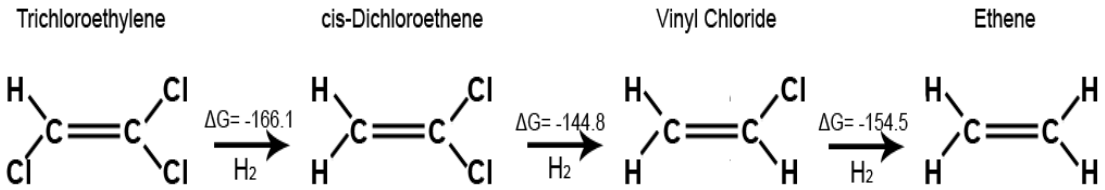

Figure 1.1 – Reductive dechlorination of TCE and its daughter species. Gibbs free energy values are from Dolfing (2000) and are listed in KJ/mol.[14]

Only ethene exists as a non-toxic endpoint, since cis-DCE has a toxicity similar to that of TCE, and VC is known to be extremely dangerous and carcinogenic.[15,16] Therefore, complete dechlorination is necessary for adequate remediation. However, these reactions are slow in most natural environments. Abiotic degradation via hydrolysis is extremely slow and often ignored, with half-lives as long as 10^6 or 10^8 years.[2,3] Aerobic biodegradation via oxidation is often considered insignificant as well, with slow reaction rates and an unlikelihood of complete dechlorination.[4,5] Anaerobic biodegradation via reductive dechlorination, however, has been shown to significantly degrade TCE to ethene in some natural settings.[2-5]

1.2 Anaerobic Biodegradation of Trichloroethylene

Anaerobic dechlorination of TCE can occur via one of three distinct biological pathways. The first pathway is through the use of chloroorganic compounds as both carbon and energy sources. Although this reaction can successfully degrade TCE, its occurrence in natural systems is extremely uncommon, as only a select group of organisms are known to be involved.[17,18] Instead, most organisms use cometabolic pathways for biochemical transformation. Cometabolism involves the indirect modification of a compound by enzymes or cofactors that normally catalyze other

reactions. In the case of TCE, methanogens and sulfate reducers are arguably the most prevalent groups involved due to their abundance in most anaerobic systems and diversity of species that can participate in reductive dechlorination.[18] During methanogenic-coupled reductive dechlorination, TCE is reduced by hydrogen released from methyltransferase and methyl-coenzyme M reductase activity. Similarly, in sulfate reducers, sulfite reductase activity releases hydrogen, which catalyzes the reductive dechlorination of TCE through the electron carrier ferredoxin. Although these cometabolic reactions are common in natural systems, their rates are often slow.[17] Processes that are energetically useful for the cell are typically more effective at degrading TCE.

Dehalorespiration is the last biochemical pathway involved in the transformation of TCE. This process uses halogenated compounds as electron acceptors for microbial growth. More specifically, electrons are transferred from hydrogen to TCE during the synthesis of ATP through chemiosmosis. As a direct result of this electron transfer, TCE is reductively dechlorinated to DCE.[17,18] A schematic diagram for this process is depicted below.

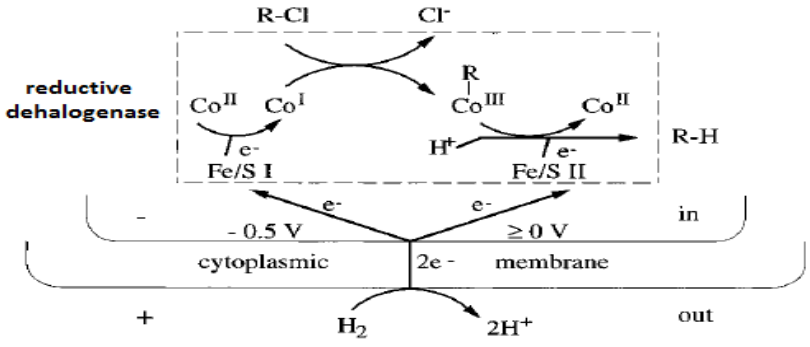

Figure 1.2 – Depiction of the processes involved in dehalorespiration. The dechlorination reaction is catalyzed by a reductive dehalogenase enzyme that contains cobalt-corrinoid factors (Co) and iron-sulfur clusters (Fe/S). Image taken from Fantroussi et al. (1998) with minor alterations.[17]

Recently, the *Dehalococcoides* group of bacteria has been implicated in the dehalorespiration of TCE. This genus, which is not closely related to any other microbial class, has become central to the study of reductive dechlorination. It contains the only known organism (*Dehalococcoides ethenogenes* 195*)* that can completely dechlorinate TCE to ethene via a respiratory process.[19-21] The rate of this reaction is typically much quicker than cometabolic processes (provided that conditions are anaerobic and there is sufficient hydrogen, acetate, and vitamin B12 to sustain growth).[21] The reaction rate is also affected by a number of other factors. Typically, it increases with increasing strength of reducing conditions,[3,4,22] abundance of electron shuttles (i.e. natural organic matter),[4,17] number of chlorine atoms on the chemical,[4,22] and quantity of microorganisms involved in dechlorination.[3,19] However, if conditions are unfavorable towards reductive dechlorination, or if the extent of contamination is too high, then engineered solutions are often required for remediation.

1.3 Engineered Remediation of Trichloroethylene Using Zero-Valent Iron

The United States government spends billions of dollars annually on traditional remediation methods for TCE contaminated superfund sites. The most common of these is the "pump-and-treat" method, which works by pumping water from the contaminated site into a storage basin, heating and/or stirring the water to promote volatilization of the harmful chemicals, and returning the treated water via another system of pumps.[23] This method is inherently inefficient, invasive, and expensive for cases of groundwater contamination.[23,24] Therefore, less expensive *in*

situ remediation methods are increasing in popularity. One such method is the installation of a permeable reactive barrier, which is filled with a chemical medium that reacts with and degrades contaminants as water flows through the system.[25] This chemical medium can also be injected into the contaminated water through a method referred to as direct injection. This reduces installation costs by eliminating the need for a barrier.[23] In either case, zero-valent iron (ZVI) has emerged as a relatively cheap and effective chemical medium for contaminant remediation, including TCE dechlorination.[25-28]

ZVI enhances the degradation of TCE and other chlorinated contaminants by acting as an electron donor. The pollutant adsorbs onto the surface of the iron, Fe(0) is oxidized to Fe(II) as electrons are transferred to the chlorinated chemical, the pollutant is reduced, and a chlorine atom is removed. When this reaction goes to completion, chlorine and ethene remain as non-toxic end points, and the water is effectively remediated.[29] Because this reaction is believed to be surface-mediated, zero-valent iron nanoparticles (nZVI) are often used over macro-scale iron (bulk Fe) due to the increased specific surface area and enhanced reactivity.[28-31] However, many problems exist with this new technology. Due to the highly reactive nature of these particles, oxygen exposure can cause passivation from the formation of an iron oxide surface layer.[32-35] Furthermore, when nZVI is injected into contaminated groundwater, the particles tend to aggregate, which decreases the surface area and reduces reactivity.[31,36] The addition of a polymer surface modifier addresses these issues by protecting the outer iron shell from oxidation and increasing the repulsive

forces between particles.[36-39] Nevertheless, other issues remain, such as the potential toxicity these particles could exhibit on ecosystems and human health.[40,41]

1.4 Potential Toxicity of Zero-Valent Iron Nanoparticles

Despite the growing popularity of nanoparticles, there are still many unknowns when considering their toxic effect. Information regarding the health and environmental risk of manufactured nanoparticles is lacking, and no single parameter has been established as the source of biological damage.[42,43] Physical and chemical characteristics (i.e. composition, size, surface area, zeta potential, etc.) may all play unique roles in the manifestation of toxicity.[43-46] Therefore, it is difficult to generalize or predict the potential risks of nanoparticles in the environment.

Regarding nZVI toxicity specifically, recent research has revealed an apparent bactericidal effect during exposure to different microbial populations under varying conditions.[41,47-51] The following studies are of particular importance. Lee et al. (2008) found a linear response between the inactivation of *E. coli* and nZVI dose in the absence of oxygen, with a bactericidal activity "comparable to that of silver nanoparticles". Furthermore, no significant bactericidal effect was observed for other iron-based compounds, such as iron powder or ions, suggesting a unique nanoparticle-based toxicity.[48] Xiu et al. (2010) observed a similar bactericidal effect for bare nZVI during exposure to *Dehalococcoides* microbial communities. The researchers detected significant down regulation of the *tceA*, and *vcrA* genes, which are responsible for dechlorination activity.[49] Lastly, Fajardo et al. (2012) observed dose- and species-dependent nZVI toxicity during exposure to soil microcosms. In

summary, they found limited morphological changes, but significant changes to the phylogenic composition of the microbial community.[50]

These three studies demonstrate the potential damage nZVI could have on microbial communities when used for groundwater remediation. If the bactericidal effect is strong enough, then nZVI could inhibit long-term contaminant degradation by inactivating microbes responsible for dechlorination. However, it is unknown whether the bactericidal properties of nZVI will have any effect on microbial populations in complex environmental systems. Some studies have shown that dissolved oxygen and natural organic matter greatly reduce bactericidal activity via passivation of the nanoparticle surface.[51,52] Other studies have shown that nanoparticle surface coatings exhibit a similar passivation effect, with coated nZVI displaying little to no bactericidal activity.[49,51,52] Overall, there are many unknowns surrounding nZVI toxicity. The general consensus is that more studies are needed to evaluate the potential toxicity of bare and coated nZVI to naturally occurring microbes in different settings.[31,40,53,54]

1.5 Research Questions and Experimental Overview

This study attempts to address some of the questions and contradictions involving nZVI microbial toxicity. Most significantly, it is still unclear as to whether these particles will exhibit the same toxicity in natural systems as that observed in laboratory studies using deionized water and agar. Furthermore, the source of this observed microbial toxicity is still unclear. Some studies have suggested a unique nanoparticle-based effect, while others have proposed alternative factors (i.e. iron

ions and oxidant generation). Finally, most studies examine only one type of iron nanoparticle, but there is evidence that bare and surface-modified particles can possess different toxic potentials. Therefore, this study compares the toxicities of bare nZVI, coated nZVI, and bulk Fe in laboratory conditions mimicking a TCE-contaminated groundwater environment and attempts to discern the source of toxicity.

The experimental procedures used to accomplish this task are depicted in Appendix A and are summarized briefly. An anaerobic enrichment culture was created using groundwater from a TCE-degrading microcosm. This culture was then transferred into separate vials and spiked in triplicate with either additional culture (for the experimental blank), modified DI water (for the negative control), silver nanoparticles (for a positive control), bare nZVI, coated nZVI, or bulk Fe. Aliquots were taken, pH and ORP were measured, RNA was extracted, and cDNA was synthesized for each of the experimental samples. The cDNA was then analyzed with qPCR for *Dehalococcoides* spp., total Bacteria, total Archaea, methanogen, and sulfate reducing bacteria populations. The results were evaluated using a Welch ANOVA to test for statistically significant differences between the experimental treatments. Microbial toxicity was determined via comparison to the blank and negative control. Finally, these findings were used to assess for possible relationships between microbial response and nanoparticle characteristics, ion release, and water chemistry.

Chapter 2: Materials and Methods

2.1 Sample Collection

Soil samples used in this study were taken from the saturated zone portions (2-12 ft. in depth) of soil borings collected from a TCE contaminated superfund site (Beaverdam Road Landfill) on the Beltsville Agricultural Research Center (BARC). These borings were collected by BMT Entech in March 2011 and stored in a freezer until use. Groundwater samples were collected in December 2012 from the same site using monitoring wells previously established by BMT Entech. All water samples were stored at 2°C prior to use. For a detailed description of the superfund site, TCE contamination, boring and monitoring well locations, and soil and groundwater characteristics, please refer to the final report by BMT Entech (2008).[55]

2.2 Microcosm Preparation

Three soil-groundwater and three sand-groundwater microcosms were created as part of a larger experiment for testing the effectiveness of different biowall compositions on the remediation of TCE. These microcosms were prepared in sterile 1-L jars, which contained roughly 500 mL solids (either site soil or autoclaved concrete sand) and 250 mL site groundwater. The jars were evacuated, and 50.0 mL TCE (Sigma Aldrich reagent grade powder in DI water, initial concentration of 600 ppb) was added for a final concentration of 100 ppb in each jar. After the TCE addition, the jars were re-pressurized with nitrogen to 16 psia. The microcosms were

then incubated in the dark at 12°C for one year to imitate groundwater conditions. Measurements were taken periodically by Maryland Spectral Services (Baltimore, MD) via GC-MS headspace analysis. The decrease in TCE concentration over time was used to assess the dechlorination activity of each jar. One of the soil-groundwater jars exhibited a TCE removal of >99.9%, as compared with an average removal of ~55% for the sand-groundwater jars. This jar was determined to contain the most active dechlorinating microbial community and was used for preparation of an enrichment culture.

2.3 Enrichment Culture Preparation

Groundwater that was previously collected from Entech Well 4 was transferred to a 1-L jar, sterilized in an autoclave (Microbiology International Systec VE-150), sparged with analytical grade nitrogen for 1 hour at 20 psi, and placed in an anaerobic chamber (COY Industries) that was filled with a gas mix of 90% N_2, 5% CO_2, and 5% H_2 (Airgas, certified standard grade). The water was then mixed overnight at 1000 rpm using a magnetic stir plate to promote gas exchange and minimize the concentration of dissolved oxygen.

Afterwards, approximately 300 mL of this groundwater was transferred to the microcosm jar that exhibited the greatest degree of dechlorination activity. The jar was then shaken vigorously for 30 min to promote transfer of the microorganisms into the aqueous phase. It was then set aside for 24 hours to allow the solids to settle. After this period, the clear liquid portion of the microcosm was pipetted into an autoclaved, 1-L culture flask. This process of adding groundwater, shaking

vigorously, settling the solids, and pipetting was repeated until a total of 500 mL of liquid had been transferred from the microcosm into the culture flask.

Next, sodium acetate (Sigma Aldrich, molecular biology grade, ≥99.0%) and TCE (Sigma Aldrich, analytical standard grade, 5000 µg/mL in methanol) were added to the culture flask for a final aqueous concentration of 10.0 mM and 0.04 mM, respectively, in an effort to enhance the *Dehalococcoides* spp. population. The flask was then stored in the anaerobic chamber at room temperature in the dark for three weeks before use in the toxicity study. Substrate addition was repeated at the two week mark for a total *added* concentration of 20.0 mM sodium acetate and 0.08 mM TCE (although the actual aqueous concentration would be less due to metabolism during storage and gaseous escape upon opening the flask). A half-dose of sodium acetate was also added immediately before the toxicity study to reduce stress on the bacteria; the final *added* concentration of sodium acetate was 30.0 mM.

2.4 Nanoparticle Preparation and Characterization

2.4.1 Commercial Supplies

Iron nanoparticles were supplied by NANO IRON, s.r.o as either an aqueous dispersion (20.0% nanoparticle weight content) stabilized by a biodegradable organic and inorganic modifier (NANOFER 25S), or an air-stable powder consisting of surface stabilized nanoparticles (NANOFER STAR). More information regarding the chemical and physical properties of these particles can be found at www.nanoiron.cz. Polyvinylpyrrolidone

(PvP)-coated silver nanoparticles (20-30 nm, 99.95% purity) were purchased from Sky Spring Nanomaterials, Inc. (Houston, TX) in the powder form.

2.4.2 Solution Preparation

For preparation of a 5 g/L silver nanoparticle solution, 500 mg of the PVP-coated silver nanopowder was accurately weighed into an autoclaved, 100-mL volumetric flask. The flask was then transferred to the COY anaerobic chamber, where it was filled to the mark with autoclaved, N_2-sparged DI water. Ethanol (Fisher Scientific, molecular biology grade, 70%) was then added for a final concentration of 4.2% (wt/wt) to help stabilize the particles. Finally, the particles were further stabilized by adding concentrated sodium hydroxide (Sigma Aldrich, reagent grade, 50% in water) drop-wise to raise the pH of the solution to approximately 10. Under these conditions, the nanoparticles exhibited settling over time, but were easily and completely dispersed into solution upon shaking for 30 seconds.

To prepare a 50 g/L bare iron nanoparticle solution, 30.0 g of the NANOFER STAR nanopowder was accurately weighed into a 500-mL beaker, which was then transferred to the anaerobic chamber. Next, 120.0 mL of autoclaved, N_2-sparged DI water was added to the beaker, and the mixture was blended at ≥10,000 rpm for 1 min. This process was suggested by the manufacturer for the activation of the particles; at this ratio and speed, the nanoparticles collide into one another, resulting in partial removal of the oxide shell. After the activation process, a volumetric pipet was used to transfer 30.00 mL of the nanoparticle slurry to a 100-mL volumetric flask. The flask

was then filled to the mark with autoclaved, N_2-sparged DI water, ethanol was added for a final concentration of 4.2%, and the pH was raised to approximately 10 using sodium hydroxide. The iron nanoparticles exhibited similar settling and re-suspension characteristics as the silver nanoparticles under these conditions.

A 50 g/L coated iron nanoparticle solution was prepared by transferring 37.50 mL of the NANOFER 25S nanoparticle slurry to a 100-mL volumetric flask inside the anaerobic chamber. The flask was then filled to the mark with autoclaved, N_2-sparged DI water, and ethanol and sodium hydroxide were added to replicate the composition and pH of the other nanoparticle solutions. The nanoparticles were extremely stable under these conditions; no settling was observed after an hour without agitation.

2.4.3 Zeta Potential Determination

Each of the nanoparticle solutions were diluted to 1 g/L in autoclaved, N2-sparged DI water. These dilutions were then used to fill three disposable capillary cells (Malvern Instruments). Zeta potential, electrophoretic mobility, and conductivity measurements were performed in a Nano ZS90 (Malvern Instruments). A refractive index of 2.42, 2.54, or 1.33 and an absorption value of 0.20, 0.20, or 0.01 were used for the bare iron nanoparticles, coated iron nanoparticles, and PVP-Ag nanoparticles, respectively.

2.4.4 Transmission Electron Microscopy

The previously prepared nanoparticle solutions were diluted to 1000 ppm in ethanol (Fisher Scientific, molecular biology grade, 70%). A 10.0 µL aliquot of each solution was then placed onto a 400-mesh copper grid coated with a thick carbon film (Pacific Grid Tech). After the grids were dry, they were then transported to the Maryland NanoCenter. Nanoparticle images were obtained by the NispLab using a JEOL JEM-2100F TEM.

2.4.5 X-ray Photoelectron Spectroscopy

Samples of the NANOFER STAR and PVP-Ag nanopowder were packed into individual 1-mL vials. A sample of the undiluted NANOFER 25S slurry was allowed to air-dry in the anaerobic chamber for several days. The resulting nanopowder was packed into a 1-mL vial, which was then sealed inside the anaerobic chamber. The three samples were then transported to the Maryland Surface Analysis Center, where XPS analysis was performed using a high sensitivity Kratos AXIS 165 spectrometer. In all cases, the samples were analyzed with high resolution XPS for metal (either Ag or Fe depending on the nanoparticle sample), carbon, and oxygen composition. Additionally, the bare and coated nZVI samples were analyzed for silicon and sodium composition, corresponding to components in common surface stabilizers. The bare and coated nZVI samples were also examined with four ion sputtering surveys to analyze the composition profiles in relation to nanoparticle surface depth.

2.5 Toxicity Study

2.5.1 Enrichment Culture Spiking

The 1-L flask containing the previously prepared enrichment culture was placed on a magnetic stir plate and mixed continuously at 1200 rpm to create a vortex. Volumetric pipets were then used to transfer 22.50 mL of culture into each of eighteen sterilized 50-mL crimp cap vials. Next, the vials were spiked with 2.50 mL of one of six solutions. The different treatments included a blank (additional enrichment culture), a negative control (N_2-sparged and autoclaved DI water, 4.2% ethanol, pH 10), a positive control (5 g/L PVP-Ag nanoparticles), bulk Fe [negative control water + 125 mg iron filings (Fisher scientific, -70 mesh, >99% purity)], bare nZVI (50 g/L NANOSTAR bare iron nanoparticles), and coated nZVI (50 g/L NANOFER surface-modified iron nanoparticles). Each treatment was performed in triplicate. This resulted in a concentration of 5 g/L for each of the iron treatments, corresponding to the median dose commonly applied for nZVI groundwater remediation.[53] The same concentration could not be used for the PvP-Ag NPs treatment due to decreased particle stability, so the value was reduced by a factor of 10. After spiking, the vials were sealed with crimp caps and stored in the anaerobic chamber at room temperature.

2.5.2 Solution Sampling

During sampling of a solution, the pH and redox potential of a 2 mL aliquot were measured with a Thermo Scientific Orion Dual Star pH/ISE Meter using a low maintenance pH electrode (Thermo Scientific, Orion) and a

low maintenance Redox/ORP/Temp epoxy triode (Thermo Scientific, Orion, Ag/AgCl internal reference with Pt redox sensor). These measurements were performed in triplicate, and the solution was discarded after use. Additionally, 5.00 mL of the solution was transferred into a labeled, sterile centrifuge tube. The microbial cells were pelleted in a Sorvall RC 6+ centrifuge (Thermo Scientific) for 10 min at 5,500 xg at 4°C. The supernatant was then discarded and 350 µL of a 100:1 mixture of lysis buffer RLT (Qiagen RNeasy Mini Kit) and β-mercaptoethanol (Fisher Scientific, 14.3M) was added to the tube. The tube was vortexed vigorously for 5 seconds, and the resulting suspension was transferred to a sterile 2-mL safe-lock tube with 25-50 mg glass beads (Fisher Scientific, 425-600 µm, acid-washed). Next, the microbial cells were disrupted and homogenized in a FastPrep-24 (MP Biomedicals) at 5.5 m/s for 1 min. The safe-lock tube was then centrifuged for 10 sec at max speed in a Legend Micro 21R centrifuge (Thermo Scientific). The resulting supernatant was transferred into a new sterile 2-mL safe-lock tube, which was stored at 2°C for future RNA extraction. This sampling procedure was performed for six representative samples of the enrichment culture for use as the three test samples and three time-zero measurement points. For the 24, 72, and 168 hr time points, this procedure was performed for each of the samples (three replicates for each treatment).

2.5.3 RNA Extraction

RNA extraction was performed for all samples within 24 hours of disruption and homogenization by following the Qiagen supplementary

protocol for *Purification of total RNA from Bacteria using the RNeasy Mini Kit* (RY26 Nov-06).[56] To summarize briefly, all necessary materials (excluding reagents and samples) were placed inside a UV PCR Workstation (UVP) and sterilized with UV light for 30 minutes. After this time, all materials and surfaces were cleaned thoroughly with RNase*Zap* Wipes (Ambion). Next, 350 µL of ethanol (Thermo Scientific, molecular biology grade, 70%) was added to each of the disrupted and homogenized samples, and the resulting lysate was transferred to a supplied RNeasy Spin Column in a 2-mL collection tube. The tubes were then centrifuged for 15s at 10,000 rpm in a Legend Micro 21R centrifuge (Thermo Scientific), and the resulting flow-through was discarded. Next, the columns were washed with three cycles of buffer addition, centrifugation, and flow-through removal using the supplied Buffer RW1 and Buffer RPE solutions. After the final wash step, the columns were transferred to new 2-mL collection tubes (supplied), and were centrifuged for 1 min at 10,000 rpm to eliminate any possible ethanol carryover. Finally, RNA was eluted by transferring the columns to new 1.5-mL collection tubes (supplied), adding 50 µL of RNase-free water (supplied), and centrifuging for 1 minute at 10,000 rpm. The resulting RNA pellets were resuspended via gentle mixing. Then, the RNA solutions were transferred to individual 1-mL CryoClear tubes (Globe Scientific, sterile, RNase/DNase/ ATP/Human DNA-free), which were stored at -80°C for future cDNA synthesis.

2.5.4 cDNA Strand Synthesis

Complimentary DNA (cDNA) was synthesized from the extracted RNA for each sample using RevertAid H Minus First Strand cDNA Synthesis Kits (Thermo Scientific). The reactions were performed according to the manufacturer's instructions, which are summarized briefly below.

All necessary materials (excluding reagents and samples) were placed inside the UV PCR Workstation and sterilized with UV light for 30 minutes. Afterwards, all materials and surfaces were cleaned thoroughly with RNase*Zap* Wipes. A master mix was then prepared on ice by transferring the required amounts of 5X Reaction Buffer, RiboLock RNase Inhibitor, 10 mM dNTP Mix, RevertAid H Minus M-MuLV Reverse Transcriptase, Random Hexamer Primers, and Nuclease-Free Water (all supplied) for a total volume of 50 µL per cDNA synthesis reaction. The master mix was then mixed gently via pipetting, spun down to remove bubbles, and stored on ice.

Next, 35 µL of master mix was transferred into each well of a 96-well twin-tec real-time PCR plate (Eppendorf, PCR clean) placed into a 0°C PCR plate cooler (Eppendorf). The plate was then covered with adhesive PCR film (Eppendorf, PCR clean), spun down for 20 seconds in a PCR plate spinner (Labnet MPS 1000), and returned to the PCR plate cooler. Afterwards, 15 µL of template was transferred into each well of the plate. The template consisted of either extracted RNA for each of the experimental samples, extracted RNA for three test samples, or nuclease-free water for the no template control.

Additionally, an RT- control was prepared by transferring all of the individual master mix components (excluding the RevertAid H Minus M-MuLV Reverse Transcriptase) into a separate well on the PCR plate and adding 15 µL of RNA template from one of the test samples. This was done to ensure there was no genomic DNA contamination in the extracted RNA samples.

The completed reaction plate was then placed inside a thermal cycler (Eppendorf Mastercylcer realplex^2) and was run for 5 minutes at 25°C, 60 minutes at 42°C, and 5 minutes at 70°C. After this time, the resulting cDNA synthesis products were quantitatively transferred to 1-mL CryoClear tubes and diluted with the supplied nuclease-free water (1:2 dilution, cDNA product: H_2O). The cDNA products for the test samples, no template control, and RT- control were stored at -20°C for future cDNA reaction verification. The cDNA products for the experimental samples were stored at -80°C for future qPCR sample analysis.

2.6 Quantitative Polymerase Chain Reaction Analysis

2.6.1 Preparation of Standards

Linearized and purified plasmid DNA standards for Bacterial and Archaeal 16S rRNA, dissimilatory sulfate reductase, and methyl coenzyme M reductase were supplied by Dr. Stephanie Yarwood (University of Maryland – Environmental Science & Technology Department). The concentration of each standard was determined using a Qubit dsDNA BR Assay with a Qubit

1.0 fluorometer (Invitron). The plasmids were stored in Tris buffer (10 mM Tris-HCl pH 8.5) at -20°C.

A plasmid DNA standard for *Dehalococcoides* spp. 16S rRNA was obtained from a culture streaked onto an LB/AMP agar plate that was supplied by Cynthia Swift from Dr. Frank Loeffler's lab (University of Tennessee – Microbiology Department). This culture consisted of *E. coli* with plasmids cloned from a *Dehalococcoides* sp. BAV1 strain using primers 8F/1429R inserted into the pCR2.1 vector with TOPO 10 chemically competent cells.

To extract the plasmids, liquid cultures of the *E. coli* were prepared from the provided agar plate. In short, two sterile tubes were placed in a UVP Sterilizing PCR Workstation and were filled with LB solution. An isolated colony was then selected, and a portion was transferred from the agar plate to each of the LB tubes using sterile inoculating loops and flame aseptic techniques. The tubes were then closed loosely and placed in a shaker at 37°C for 24 hours. After this time, plasmid DNA was extracted from the two culture tubes using a GenElute HP Plasmid MiniPrep Kit, and the concentration was determined using a Qubit dsDNA BR Assay with a Qubit 1.0 fluorometer (Invitron). Finally, plasmid standards were stored in the supplied elution solution (10 mM Tris-HCl pH 8.5) at -20°C.

Serial dilutions of each plasmid standard were created for use as qPCR standard curves. First, the stock solution of plasmid standard was allowed to thaw at 2°C, after which the solution was vortexed for 20 seconds. Next, four 1:100 serial dilutions were prepared on ice by transferring 2 µL of standard

into a 2-mL safe-lock tube (Eppendorf, PCR clean) with 198 µL of UltraPure water (Invitrogen, molecular biology grade, DNase/RNase-free). The dilutions were then vortexed for 20 seconds and centrifuged for 10 seconds at 4000 rpm to spin down the contents and remove any air bubbles. A fifth standard was then prepared via the same process by making a 1:10 dilution of the lowest concentration standard. This process resulted in plasmid standards with concentrations on the 10^{0}, 10^{-2}, 10^{-4}, 10^{-6}, and 10^{-7} orders of magnitude (ng/µL). Gene copy numbers were then calculated using the equation in Appendix B. All standards were stored at -20°C.

2.6.2 Verification Reactions

Unless otherwise stated, all qPCR runs were executed using a Mastercylcer realplex^{2}, 96 well twin-tec real-time PCR plates, and adhesive PCR film (Eppendorf, plates and film were PCR clean). The qPCR solution was either Power SYBR Green PCR Master Mix (Applied Biosystems) for Bacterial and Archaeal 16S rRNA, dissimilatory sulfate reductase, and methyl coenzyme M reductase, or TaqMan Fast Advanced Master Mix (Applied Biosystems) for *Dehalococcoides* spp. 16S rRNA. Prior to protocol optimization, thermal cycler conditions and primer/probe concentrations were taken from the master mix protocols.[57,58] Primer sets were synthesized by Eurofins MWG Operon and are listed in the table below.

Gene	Forward primer (5' to 3')	Reverse primer (5' to 3')	Probe	Source
Bacteria 16S	Eub 338 – ACT CCT ACG GGA GGC AGC AG	Eub 518 – ATT ACC GCG GCT GCT GG	N/A	Fierer et al. (2005)[59]
Archaea 16S	A915 – AGG AAT TGG CGG GGG AGC AC	A1059 – GCC ATG CAC CWC CTC T	N/A	Yarwood et al. (2010)[60]
Dissimilatory sulfate reductase	dsrA 1 – ACS CAC TGG AAG CAC G	dsrA 500 – CGG TGM AGY TCR TCC TG	N/A	Wilms et al. (2007)[61]
Methyl coenzyme M reductase	mcrIRD F – TWY GAC CAR ATM TGG YT	mcrIRD R – ACR TTC ATB GCR TAR TT	N/A	Lever (2008)[62]
Dehalococcoides spp. 16S	Dhc1200 – CTG GAG CTA ATC CCC AAA GCT	Dhc1271 – CAA CTT CAT GCA GGC GGG	FAM-TCC TCA GTT CGG ATT GCA GGC TGA A-TAMRA	Sung (2005)[20]

Table 2.1 –Primer sets for the six qPCR assays. A TaqMan probe was only used for *Dehalococcoides* spp. 16S, because all other assays were performed using SYBR qPCR.

Primer, standard, and sample viability tests were performed for each of the target genes. These were done via qPCR of the previously prepared standard dilution series, previously synthesized cDNA from the three test samples, and no template controls. Fluorescence values were analyzed using the provided software (Eppendorf Mastercylcer ep realplex 2.2). Successful amplification of the standards and test samples with no or little amplification of the no template controls was viewed as verification for the validity of the qPCR assay. Unfortunately, no amplification was detected for the test samples when using the methyl coenzyme M reductase or *Dehalococcoides*

spp. 16S primers. Because the standards for these primers amplified in the expected range, it was concluded that the methanogen and *Dehalococcoides* spp. starting microbial populations were below the detection limit and could not be measured. As a result, these two qPCR analyses were excluded from further study.

The success of the previous cDNA synthesis reactions was analyzed via Bacterial 16S rRNA qPCR of the test samples, no template control, and RT- control. Fluorescence values were analyzed using the provided software. Successful amplification of the test samples and limited or non-existent amplification of the controls was viewed as verification for the validity of the previous cDNA synthesis reactions.

2.6.3 Protocol Optimization

The reaction conditions of primer concentration, annealing temperature, and extension time were optimized for each target gene with regards to qPCR sensitivity, linearity, and efficiency. First, the optimum primer concentration was determined according to chapter four of the Power SYBR Green PCR Master Mix User Guide. To summarize briefly, nine PCR master mixes were created with all possible combinations of 50, 300, and 900 nM forward and reverse primer concentrations. Next, 18 µL aliquots of the various master mixes were transferred into individual wells in a 96 well plate. Finally, 2 µL of either positive (1-10 ng plasmid DNA) or negative (nuclease-free water) template was transferred into each well. The resulting reaction plate contained triplicates of both positive and negative controls for

each of the primer concentration combinations. The plate was then placed into the thermal cycler and run with the standard qPCR conditions listed in the user guide. The reaction with the smallest primer concentration that had both a low threshold cycle (Ct) for the positive control and a very high or absent Ct for the negative control was chosen as the optimum primer combination (see Appendix C for values).

The optimum annealing temperature and extension time was determined by analyzing the sensitivity, linearity, and efficiency of a standard curve. First, qPCR reactions for the previously prepared standard serial dilutions and no template controls were run using the optimized primer concentrations and the standard two step cycling conditions listed in the Power SYBR Green user guide. The results were then analyzed using the provided software. Sensitivity of the assay was determined to be the lowest concentration of standard that had a significantly smaller Ct value than the no template controls. Linearity was determined from the regression of the standard curve, and efficiency was determined from the slope; both were calculated using Eppendorf's built-in CalQplex algorithm. Annealing temperature was then reduced by 2-5°C, and the qPCR reactions were repeated using a three step cycle (denature for 15 seconds at 95°C, anneal for 30 seconds at X°C, and extend for 30 seconds at 60°C). This process was repeated until the value resulting in optimum sensitivity, linearity, and efficiency was discovered. If a single value could not be found to optimize all of the qPCR properties, then sensitivity was preferentially selected over

efficiency. Next, extension time was increased by 10s, and the qPCR reactions were repeated using the optimized annealing temperature. Again, this process was repeated until the value resulting in optimum sensitivity, linearity, and efficiency was discovered. These optimum settings were then used for all subsequent qPCR assays (see Appendix C for values).

2.6.4 Test for Inhibition

Because iron is a known inhibitor of qPCR reactions,[63-65] selected experimental samples believed to have the highest concentration of dissolved iron were analyzed for SYBR signal inhibition. First, the cDNA solutions of the experimental samples were separated into five categories based on hue: brown (believed to have the most iron), orange, yellow, pale yellow, and clear (believed to have little to no iron). The sample hues corresponded well with expected dissolved iron content based on the type of spiking solution used in the toxicity study. Consequently, three random experimental samples from each of the brown, orange, and yellow groups were chosen for inhibition analysis. For each of the groups, 5-µL aliquots were taken from the three random samples and pooled into a single sample. Then, serial dilutions were created from each pooled sample to create 1:2, 1:10, 1:50, 1:250, and 1:1250 dilutions in nuclease-free water.

A Bacterial 16S rRNA qPCR assay was then used to analyze the extent of inhibition in each dilution. The test was performed with three replicates of each of the following: serial dilutions for each group, the same serial dilutions spiked with a known amount of Bacterial 16S rRNA plasmid standard,

nuclease-free water spiked with the same amount of standard, Bacterial 16S rRNA standard curve, and no template controls. The fluorescence data was analyzed with the provided software, and the standard curve was used to calculate gene copy numbers for each sample. The difference between the expected concentration in the spiked samples (calculated from the summation of the gene copy numbers in the corresponding un-spiked dilution and the spiked water control) and the observed concentration in the spiked samples (calculated from the fluorescence data) was used to determine the degree of inhibition in each serial dilution. Significant inhibition was observed for each group. A 1:10 dilution was sufficient to prevent inhibition of the yellow group, whereas 1:50 and 1:1250 dilutions were required for the orange and brown groups, respectively.

This inhibition test was then repeated with the addition of bovine serum albumin (BSA). BSA has been shown to significantly reduce the inhibitory effects of iron in qPCR assays.[66] Therefore, 0.4% (wt/vol) BSA (Thermo Scientific Fermentas, 20mg/mL BSA in Tris-HCl, molecular biology grade, DNase/RNase-free) was added to the SYBR master mix, and each of the previously described samples were analyzed using a Bacterial 16S rRNA qPCR assay. The fluorescence data was examined with the provided software, and the degree of inhibition was calculated as previously described. A 1:2 dilution ratio with 0.4% BSA resulted in the lowest threshold cycles with no evidence of qPCR inhibition for any of the samples. Therefore, these conditions were used for all subsequent sample assays.

2.6.5 Analysis of Experimental Samples

Before beginning the qPCR analyses, aliquots of the reaction materials were created to avoid excess freeze-thaw cycles. This step was performed for the previously prepared cDNA samples, plasmid standard dilutions, primer sets, and BSA solutions. The aliquots were stored at -20°C until their single use in a qPCR assay. The master mix solutions were stored at 2°C to avoid freeze-thaw degradation due to repeated use throughout the assays.

Each qPCR assay was performed in the UV PCR Workstation. All equipment and surfaces were sterilized with UV light for 30 minutes. All plastic-ware was certified PCR grade (DNase/RNase-free, free of genomic DNA contamination and PCR inhibitors).

First, a master mix was prepared according to the Power SYBR Green Protocol by combining the 2X SYBR solution, forward and reverse primers, BSA, and nuclease-free water. The primer concentrations for each assay are listed in Appendix C. BSA was added for a final concentration of 0.4% (wt/vol). This master mix was then mixed gently via inversion, spun down to remove any air bubbles, and stored on ice. An 18-µL aliquot of the master mix was transferred into each well of an Eppendorf white well plate placed into an Eppendorf PCR plate cooler (0°C). The plate was then covered in PCR film, and the contents were spun down in the PCR plate spinner for 20 seconds. Next, 2.0 µL of either cDNA, plasmid DNA, or nuclease-free water was transferred into each well of the plate, corresponding to the experimental samples, standards, and no template controls, respectively. Each plate was

run with four replicates of each of the following: no template control, between 9 and 12 experimental samples, and 10^{0}, 10^{-2}, 10^{-4}, and 10^{-6} ng/µL standard. Additionally, the dissimilatory sulfate reductase assays contained four replicates of a 10^{-7} ng/µL standard, due to the increased sensitivity of this assay.

The completed reaction plate was then covered with PCR film, the contents were spun down in the PCR plate spinner, and the plate was loaded into the Eppendorf Mastercycler realplex^{2}. Each assay was run using a three-step protocol with a 10 minute activation stage at 95°C, 45 PCR cycles, and a 20 minute melting curve analysis. The denaturation step was consistent across the various qPCR assays (95°C for 15 seconds). However, the annealing and extension temperatures and times varied between the target genes (see Appendix C). After conclusion of the qPCR run, the results were analyzed using the provided realplex software.

The Ct value for each of the qPCR samples was determined using Eppendorf's CalQplex algorithm and drift control settings. The melting curve was used to determine the presence of primer-dimers. Samples without a peak in the expected melting range were removed from further analysis, because the fluorescence could not be attributed to the target gene. Lastly, Ct values were corrected for varying efficiency (E) using the MultiD GenEx equation: $Ct_{(E=100\%)} = Ct_{(E)} * [\log(1+E)/\log(2)]$.[67] Although efficiency only varied by < 2% between the different runs, this correction should increase the accuracy and reliability of the statistical comparisons.

2.7 Statistical Analysis

The Ct values for each of the qPCR samples with at least three remaining replicates were examined with Dixon's Q test at the 90% confidence level. Any Ct values that were identified as outliers were rejected from further analysis. After removal of all outlying data points, the internal standard curve was used to calculate gene copy numbers (GCNs) from Ct values for the experimental samples and no template controls on each qPCR plate. In all cases, the R^2 value of the standard curve was greater than or equal to 0.98, indicating a very good linear fit. The GCNs of the replicate qPCR samples were then averaged to obtain a single value for the different target genes of each experimental sample and no template control. For experimental samples that did not amplify or for those that were excluded based on the melting curve analysis, GCNs corresponding to the lowest standard on the qPCR plate were used rather than a value of zero. This was done to reflect the detection limit of the qPCR assay and to avoid conformation bias when comparing treatments.

An ANOVA was used to test for statistically significant differences between the various treatments used in the toxicity study. The GCN for each experimental sample was entered into IBM SPSS Statistics 20. The values were then separated into six groups of three replicates each based on the type of spiking solution used in the toxicity study. Before performing a one-way ANOVA analysis, six assumptions were tested to ensure statistical validity: (1) the dependent variable must be measured at the interval or ratio level; (2) the independent variable must consist of two or more categorical, independent groups; (3) the observations must be independent of one

another; (4) there should be no statistical outliers; (5) the dependent variable must be approximately normally distributed for each categorical group; and (6) there must be homogeneity of variances.[68]

The dependent variable, GCN, is measured on the ratio level, because it consists of continuous values with a clear definition of zero. The independent variable, treatment type, consists of six groups that are mutually exclusive with an arbitrary order. Furthermore, the dependent variables were measured independently within and between the treatment types. Therefore, the first three assumptions for a one-way ANOVA are met. To satisfy the fourth assumption, Dixon's Q test was applied to the GCNs in each treatment type for the different target genes. Any value that failed the Q test at the 90% confidence level was rejected as a statistical outlier and removed from analysis. To test the fifth assumption, a Shapiro-Wilk test for normality was performed in SPSS for each treatment group. In all cases, the results were insignificant at the 90% confidence level ($p>0.10$). Therefore, the alternative hypothesis was rejected, indicating a normal distribution of data. The sixth and final assumption was examined in SPSS using Levene's test for homogeneity of variances. In all cases, the results were significant at the 90% level ($p<0.10$). Thus, the alternative hypothesis could not be rejected, and the data fails the assumption of homogeneity of variances. As a result, a one-way ANOVA could not be used to analyze the data, and a Welch ANOVA was used in its place. This test is statistically valid despite heteroscedasticity, because the means are weighted by the reciprocal of the group mean variances.[68] The Welch ANOVA was performed in SPSS using a Games-Howell post-hoc test at the 90% confidence level.

Chapter 3: Results

3.1 Nanoparticle Characterization

3.1.1 Zeta Potential

Zeta potential, electrophoretic mobility, and conductivity were determined with the provided Zetasizer Nano software (Malvern Instruments Ltd). The average values for each of the nanoparticle solutions are recorded in the table below.

Test Solution	**Zeta potential (mV)**	**Electrophoretic mobility (µmcm/Vs)**	**Conductivity (mS/m)**
PvP-Ag NPs	-38 (± 6)	-3.0 (± 0.5)	44 (± 2)
Bare nZVI	8 (± 6)	0.6 (± 0.3)	26 (± 1)
Coated nZVI	-16 (± 3)	-1.2 (± 0.2)	24 (± 1)

Table 3.1 – Zetasizer measurements for the three nanoparticle solutions: silver nanoparticles (PvP-Ag NPs), uncoated iron nanoparticles (bare nZVI), and iron nanoparticles with an organic and inorganic surface modifier (coated nZVI).

Zeta potential describes the tendency of particles to flocculate in solution. Values greater than ±30 mV are generally indicative of stable suspensions, whereas values between ±5 and ±30 are often considered incipiently unstable suspensions.[69] Electrophoretic mobility, on the other hand, is related to the ability of the charged particles to move in solution. Particles with values less than ±25 µmcm/Vs can be described as having low-charged surfaces.[69] Conductivity is simply the ability to conduct electricity

and is related to the salt content of the solution. Values between 5 and 50 mS/m are typical for most freshwater sources.[69]

3.1.2 Transmission Electron Microscopy

TEM images taken by the Maryland NanoCenter were used to determine particle size, aggregate state, and lattice structure for each of the nanoparticle solutions. Specific surface area (SSA) was calculated from the particle diameter (d) and material density (ρ), assuming a perfect sphere: SSA = surface area/mass = $6/(\rho * d)$, where ρ = 1.05E7 g/m^3 for silver and 7.80E6 g/m^3 for iron.[70] Images are displayed and explained on the following pages.

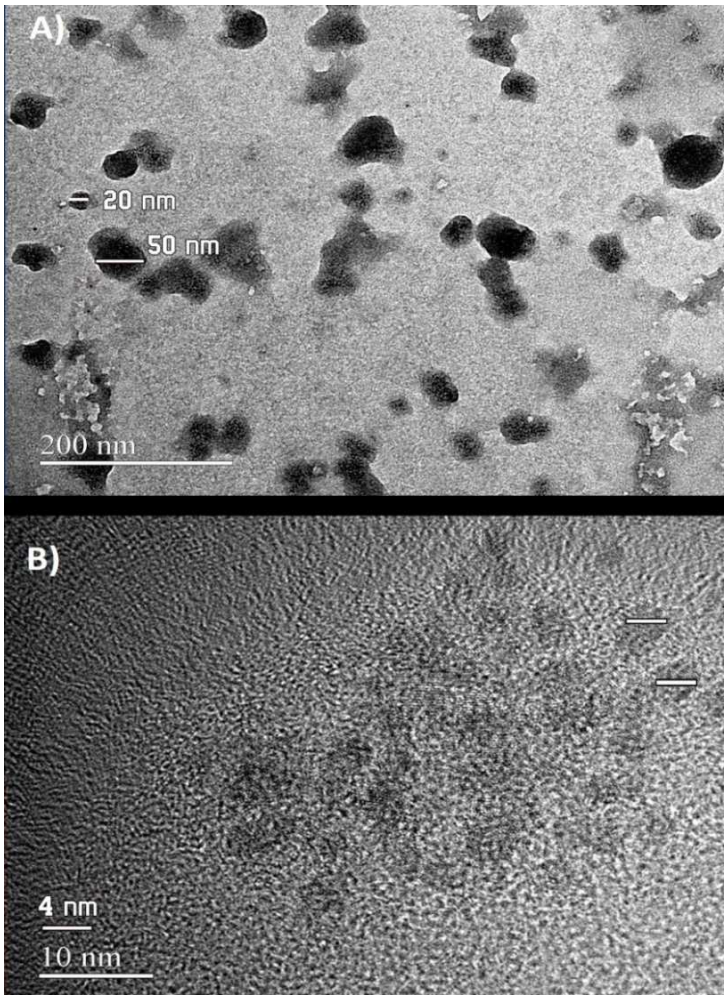

Figure 3.1 – TEM images for the PvP-Ag NPs. A) Low resolution showing the aggregate structure; B) High resolution image of an aggregate showing the lattice structure of the individual particles.

From the above TEM images, the silver nanoparticle solution appears to consist of small particles with diameters of 4 nm and specific surface areas of 143 m^2/g. These particles are crystalline in nature, and tend to form larger aggregates with diameters between 20 and 50 nm.

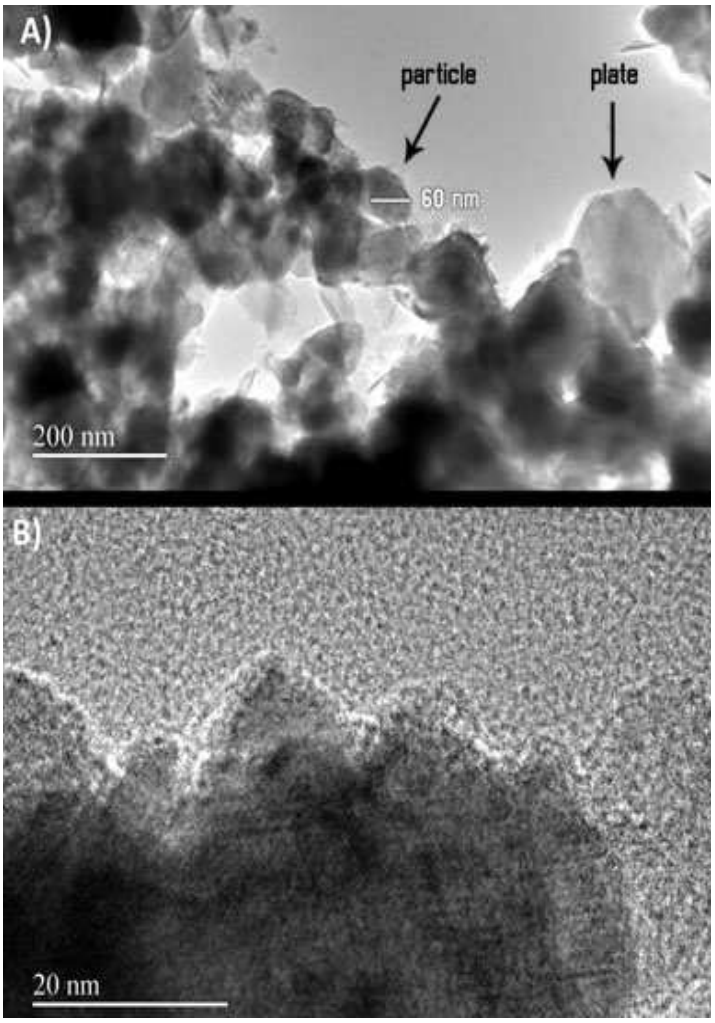

Figure 3.2 – TEM images for the bare nZVI. A) Low resolution showing the particles and aggregate structure; B) High resolution showing the lattice structure of an individual particle.

The above TEM images for the bare nZVI show individual particles with a diameter of 60 nm that are overlapping, with some forming large plate-like structures. The particles are crystalline in nature (as seen in the high resolution image) and have specific surface areas equal to 12.8 m^2/g. The plates match other descriptions seen in literature, and correspond to the formation of iron oxides.[71]

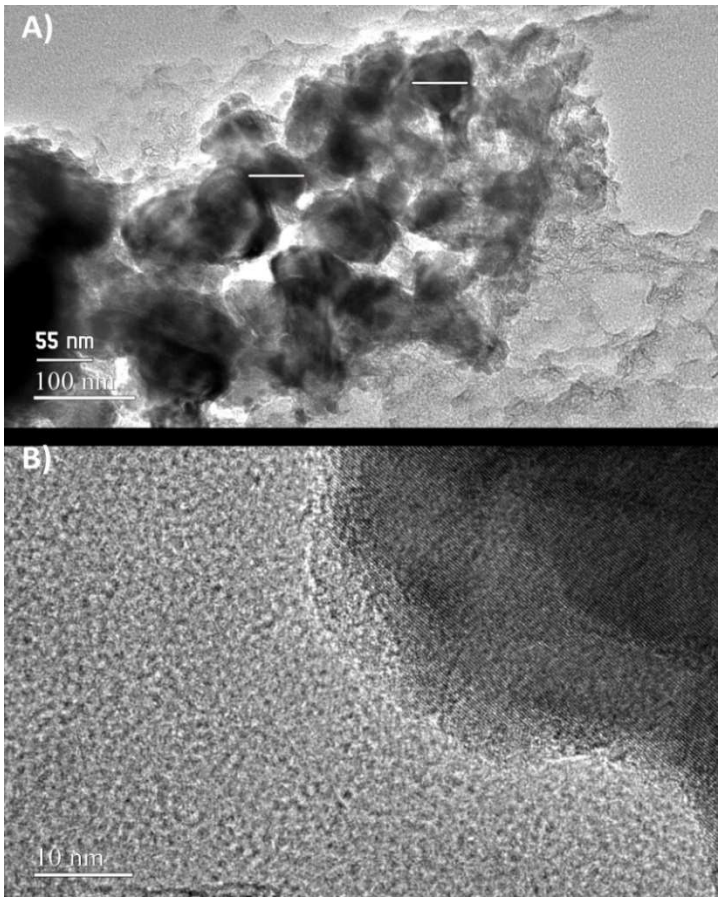

Figure 3.3 – TEM images for the coated nZVI. A) Low resolution showing the aggregate structure; B) High resolution showing the lattice structure of an individual particle.

The TEM images for the coated nZVI reveal particles with properties that are very similar to the bare nZVI. The coated nZVI particles are slightly smaller (55 nm diameter), but form similar overlapping structures. These particles are also crystalline in nature, with specific surface areas of 14.0 m^2/g. Surrounding the particles is an amorphous material, matching the description of an organic surface coating seen in a previous study.[71]

3.1.3 X-ray Photoelectron Spectroscopy

High resolution surveys and ion sputtering depth profiles from the XPS assays were provided by the Maryland Surface Analysis Center. The surveys yield detailed information regarding the particles' surface composition. The results may be seen in Appendix D, and are summarized below.

A)	**% metal**	**% C 1s**	**% O 1s**	**% Si 2s**	**% Na 1s**
PvP-Ag NPs	35.04	55.23	9.74	N/A	N/A
Bare nZVI	12.44	32.83	44.43	10.30	N/A
Coated nZVI	13.16	35.55	46.60	0.81	3.88

B)	**C 1s**			**O 1s**	
	% C-C/C-H	**% C-O**	**% COOH**	**% O^{2-}**	**% organic O**
PvP-Ag NPs	85.99	14.01	N/A	26.14	73.86
Bare nZVI	80.13	13.00	6.87	44.35	55.65
Coated nZVI	54.71	N/A	45.29	94.76	5.24

Table 3.2 – High resolution XPS data from A) particle surveys and B) element specific analyses. "% metal" corresponds to metallic Ag in the case of the PvP-Ag NPs and to Fe 2p in the case of the nZVI particles. Element specific analysis is not provided for metallic Ag, Fe 2p, Si 2s or Na 1s, because these elements only corresponded to one structure.

In the case of the PvP-coated silver nanoparticles, the above data corresponds well with spectra reported in other studies.[72,73] The surface is composed primarily of an organic modifier with some exposure to the silver

particle. Furthermore, the Ag that is present on the surface has not been oxidized and remains in the metallic state.

The bare and coated nZVI samples have very similar high resolution XPS results. The surface composition of both samples is largely organic in nature, with only a small percentage corresponding to iron. The iron on both of the surfaces corresponds well with iron oxides (likely FeO).[70] Additionally, there are only minimal amounts of metallic iron in the bare nZVI and no Fe^0 in the coated nZVI. The oxygen composition differs between the two nZVI samples. In the case of the bare nZVI, the oxygen specific analysis shows similar percentages for metallic (O^{2-}) and organic oxygen. However, the oxygen of the coated nZVI is almost exclusively metallic in nature.

Depth profile assays were performed for the two nZVI samples in an effort to better understand the core-shell structure (see Appendix E for graphs after four ion sputters). In each of the nZVI particle surveys, Fe 2p increases, C 1s decreases, and O 1s remains relatively stable with depth. The element specific analysis revealed minimal changes in the C1s composition and fluctuations between increasing and decreasing O^{2-} and organic O composition for each of the particles. The Fe 2p analysis, however, varied between the samples. In the case of the bare nZVI, ion sputtering revealed the small metallic Fe peak to increase slightly with depth, possibly corresponding to exposure of the zero-valent iron core. This did not occur in any of the coated nZVI assays. It is possible that the thickness of the surface modifications on this sample prevented detection of the Fe^0 core.[37]

3.2 Water Chemistry

3.2.1 pH

Replicate measurements for sample pH were averaged for each treatment type at the t=24, 72, and 168 hr time points; the t=0 time point corresponds to the average of three measurements of a representative sample of the enrichment culture. The data was then graphed as pH vs. time for the six treatments. Error bars represent the standard deviation of the replicates.

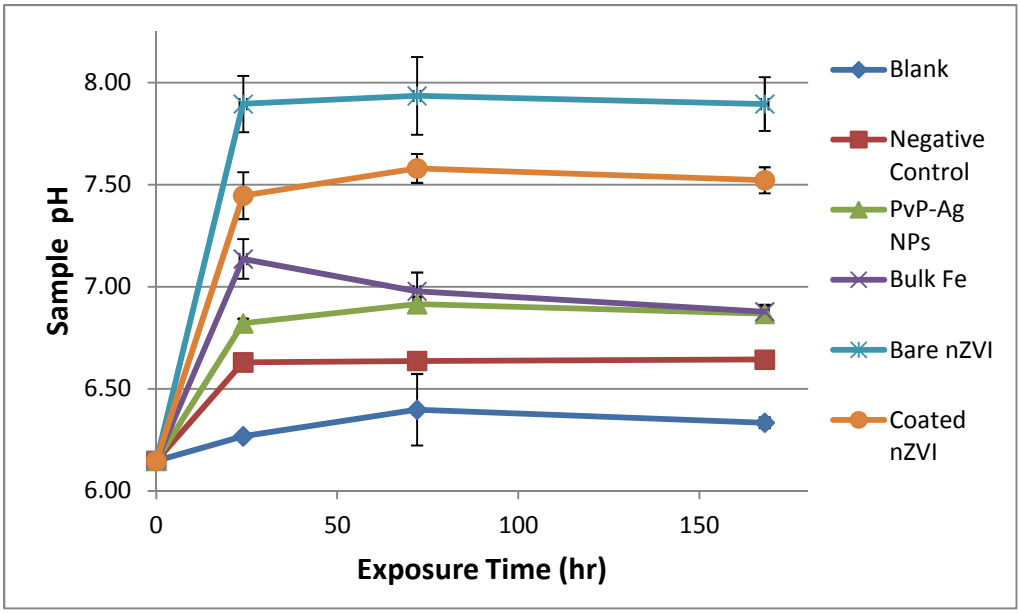

Figure 3.4 – Sample pH vs. exposure time for the six experimental treatments. For the t=0 exposure time point, the pH value was measured in triplicate using a representative sample. For the remaining time points, the pH value was measured in triplicate for each of the experimental samples after 24, 72, and 168 hours from the addition of the spiking solution. Error bars are shown, but are sometimes too small to see; they represent the standard deviation between the experimental replicates (n=3).

The starting pH of the enrichment culture was slightly acidic (6.15 ± 0.01), which is in the range of expected values for groundwater sources.[74] After 24 hours from the addition of the spiking solution, the pH value for each of the experimental treatments increased. The values then appeared to stabilize and remain relatively constant throughout the remainder of the experiment. Comparatively, the blank had the lowest pH, which is expected, because all other samples were spiked with a pH 10 solution. Conversely, the iron nanoparticle solutions had significantly higher pH values than the other treatments. In all cases, the pH values of the different treatment types were moderately similar; the range was approximately 1.5 (including the blank) or 1.0 (excluding the blank).

3.2.2 Oxidation-Reduction Potential

Sample ORP values (measured with an Ag/AgCl, sat. reference solution) were converted to standard E_h. Replicate measurements were averaged for each treatment type at the t=24, 72, and 168 hr time points; the t=0 time point corresponds to the average of three measurements of a representative sample of the enrichment culture. The data was then graphed as E_h vs. time for the six treatments. Error bars represent the standard deviation of the three replicates.

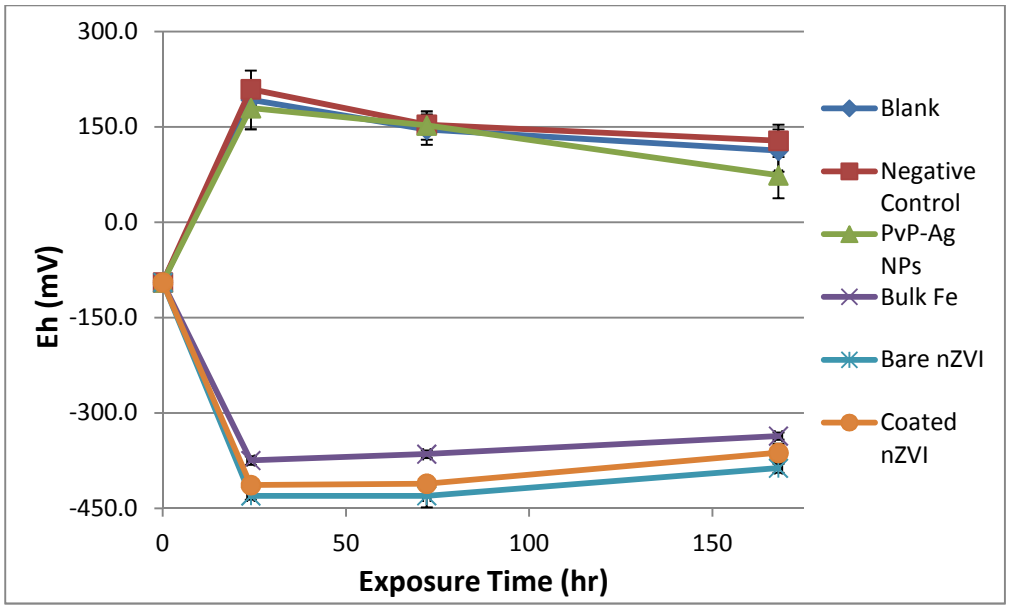

Figure 3.5 – Sample E_h vs. exposure time for the six experimental treatments. For the t=0 exposure time point, the ORP value was measured in triplicate using a representative sample. For the remaining time points, the ORP value was measured in triplicate for each of the experimental samples after 24, 72, and 168 hours from the addition of the spiking solution. Error bars are shown, but are sometimes too small to see; they represent the standard deviation between the experimental replicates (n=3).

The starting E_h of the enrichment culture was equal to -95 (±2) mV, corresponding to a reducing environment that is in the range of expected values for groundwater.[74] The reduction potential of the blank, negative control, and PvP-Ag NP treatments were between +50 and +250 mV throughout the entirety of the experiment, indicating an oxidizing environment. There was no significant difference between these samples at any of the time points based on their standard deviations. In contrast, the reduction potentials of the three iron samples were between -300 and -450 mV, indicating a highly reducing environment. In all cases, the iron

nanoparticle samples had significantly lower redox potentials than the bulk Fe. Additionally, the bare nZVI treatment had lower E_h values during the t=24 and t=168 hr time points. Based on the standard deviations, this difference was not significant at t=72. Overall, the iron treatments caused a drastic decrease in the redox potential when compared with the other samples.

3.3 Microbial Enumeration

The GCNs from the experimental samples (see section 2.7) were converted to gene copies/mL culture using the equation in Appendix F. The values of the experimental replicates were then averaged to produce a single value for each target gene at each time point for each treatment type. For example, a single gene copies/mL culture value was assigned for Eubacteria 16S measured at 24 hours after treatment with the negative control. These values were then graphed as concentration vs. time for the different target genes. Error bars were determined from the standard deviation of the experimental replicates (n=3 in all cases, except for the negative control in the Eubacteria and Archaea 16S rRNA assays, where n=2 due to the removal of a statistical outlier). The standard deviations were approximately 1 to 1.5 orders of magnitude less than the average values of the samples. This finding is relatively consistent between the different samples and time points, so it is likely a reflection of the various procedural errors during experimentation. Because the *Dehalococcoides* spp. and methanogen microbial populations could not be measured with the qPCR assays, microbial enumeration results are only presented for the total Bacteria, total Archaea, and sulfate reducing bacteria groups.

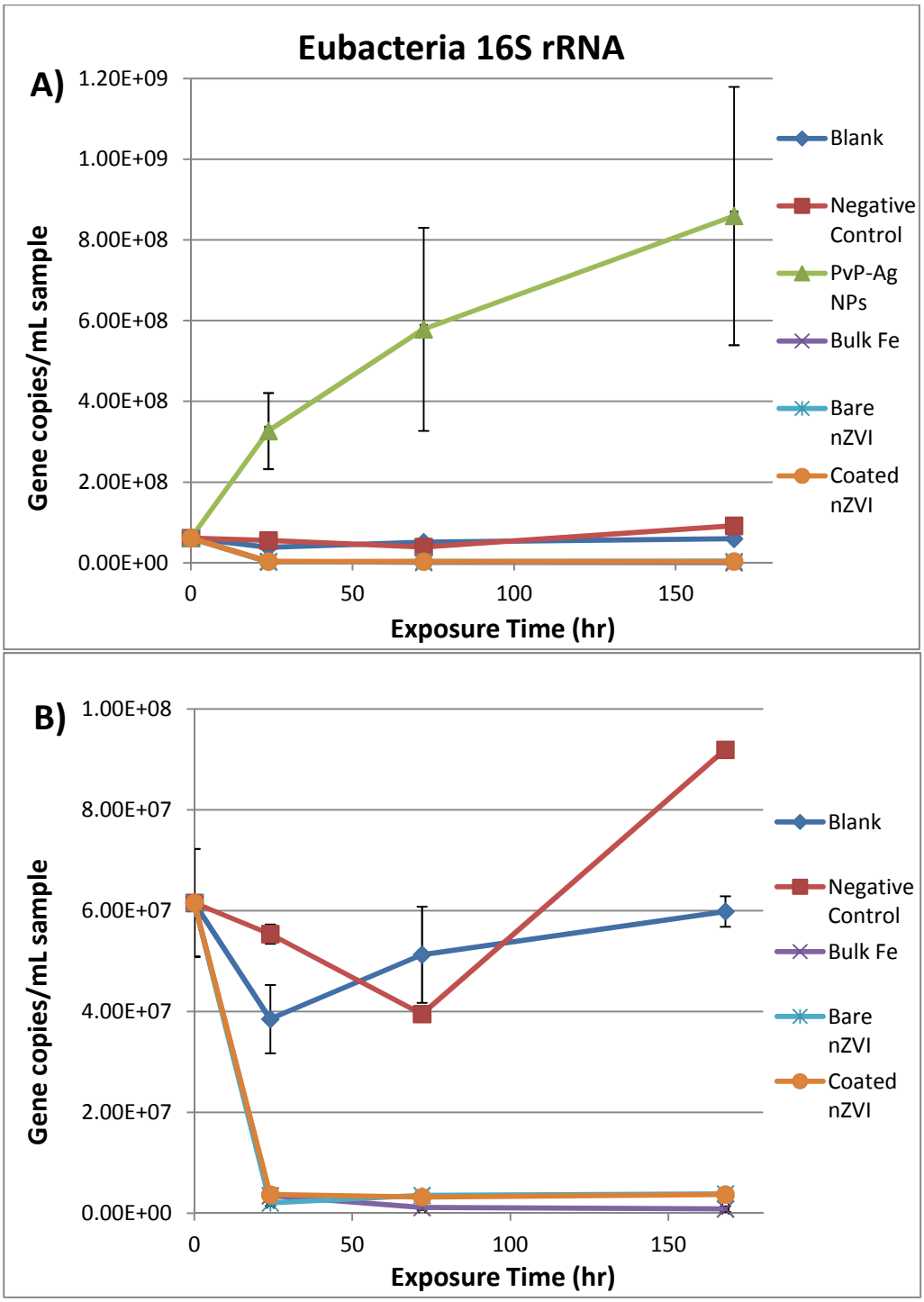

Figure 3.6 – Eubacteria 16S rRNA gene copies/mL culture vs. exposure time for the different experimental treatments. A) All samples displayed on the same scale. B) Magnification of the same graph to show differences between the samples. Error bars are shown, but are sometimes too small to see; they represent the standard deviation between the replicates.

Ribosomal RNA transcription determines the rate of ribosome synthesis. Therefore, increases in rRNA can be related to microbial growth, rather than expression of a specific cellular function.[75,76] Furthermore, the 16S portion of the rRNA is highly conserved among different species of bacteria and archaea. Primers targeting a specific portion of this gene are capable of acting as universal bacterial or archaeal amplifiers.[77,78] By measuring changes in the Eubacteria and Archaeal 16S rRNA gene copy number, we can determine how the total Bacteria and Archaea populations change over time and across treatments. Increases and decreases in this GCN can be linked to microbial growth and death, respectively.

For the total Bacteria population in the samples, most microbial death occurred within 24 hours after addition of the spiking solution. Microbial growth, however, was gradual and occurred throughout the entirety of the experiment. The only treatment that resulted in significant bacterial growth was the PvP-Ag NPs, which was surprising, because this treatment was originally designed to be a positive control for microbial toxicity. Samples spiked with this solution experienced an average GCN increase of 1.1 logs. Comparatively, results from the blank and negative control were relatively consistent over time; the GCNs increased by less than 0.2 logs after 168 hours. All of the iron-spiked samples experienced similar trends and decreases in GCN (1.2-1.8 logs). This data suggests that each of the iron treatments resulted in substantial bacterial death.

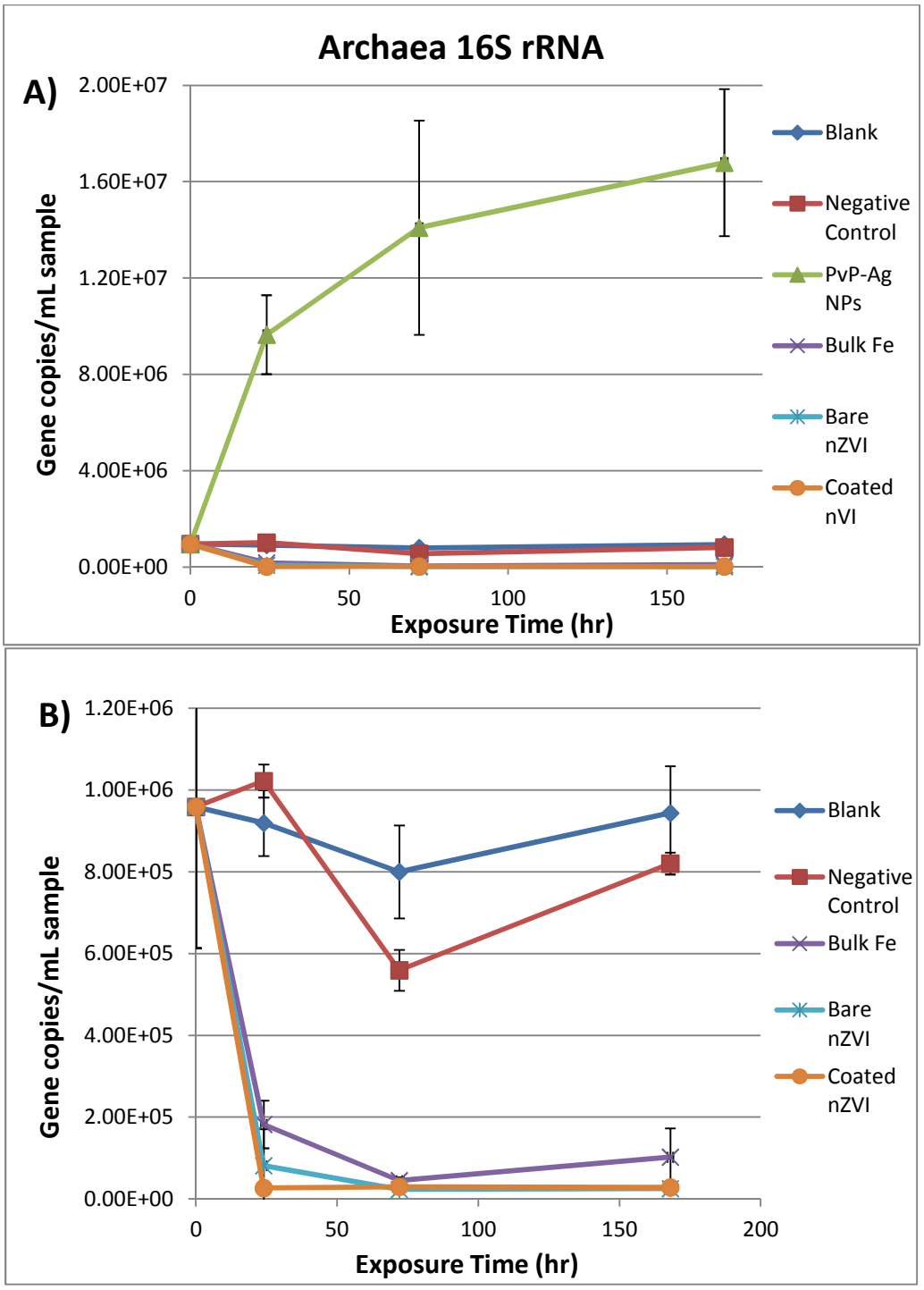

Figure 3.7 – Archaea 16S rRNA gene copies/mL culture vs. exposure time for the different experimental treatments. A) All samples displayed on the same scale. B) Magnification of the same graph to show differences between the samples. Error bars are shown, but are sometimes too small to see; they represent the standard deviation between the replicates.

The total Archaea populations in the samples experienced very similar trends in microbial growth and death as compared with the Eubacteria 16S rRNA assay. The only noticeable difference was the extent of GCN variation. The PvP-Ag NP treatment resulted in a slightly greater increase (1.2 logs), the blank and negative control were closer to the t=0 point (less than 0.005 logs difference after 168 hours), and the iron samples caused a slightly smaller decrease (1.0-1.5 logs). Additionally, the bulk Fe resulted in slightly less microbial death than the iron nanoparticle treatments, where the opposite was true for the Eubacteria assay.

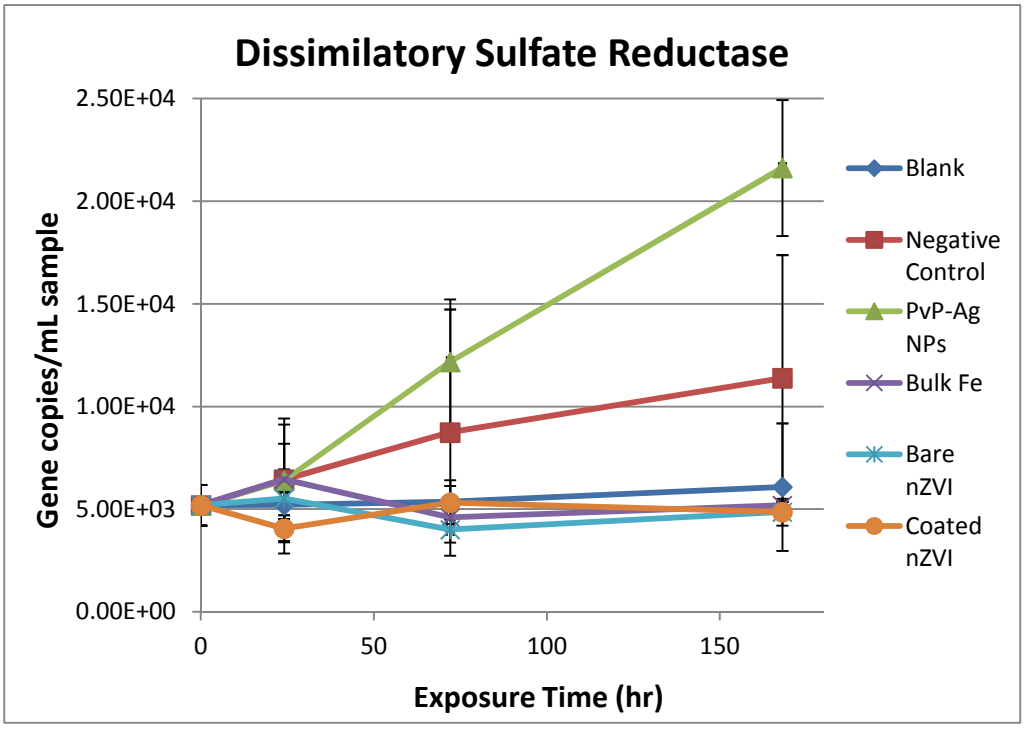

Figure 3.8 – dsrA gene copies/mL culture vs. exposure time for the different experimental treatments. Error bars are shown, but are sometimes too small to see; they represent the standard deviation between the replicates.

Unlike the Eubacteria and Archaea 16S rRNA genes, the gene used for assessing dissimilatory sulfate reductase is not directly related to microbial population. Instead, dsrA corresponds to a key functional gene involved in sulfate reduction.[61] Therefore, changes in this GCN reflect changes in sulfate reduction activity of the culture; this does not necessarily indicate an increase or decrease in the sulfate reducing bacterial population. The dsrA qPCR results revealed similar trends in GCNs as both the total Bacteria and total Archaea assays. The differences between the experimental treatments, however, are much less pronounced. For example, the PvP-Ag NPs only increased the dsrA concentration by 0.6 logs, and the iron samples only decreased it by 0.1 logs. It also appears that these differences may not be statistically significant. The ANOVA analysis was used to address this possibility.

3.4 Analysis of Variance

Nine Welch ANOVA tests were performed consisting of GCNs from the six treatment groups. These nine tests correspond to the three target genes (Eubacteria 16S, Archaea 16S, and dissimalatory sulfate reductase) measured over three time points (24, 72, and 168 hours). Statistically significant differences between the treatment types for each target gene were determined by analyzing the p-values from the Games-Howell post-hoc tests. A value of less than 0.10 was viewed as significant, indicating a statistical difference between two treatments at the 90% confidence level. Results are presented in Appendix G and are summarized below.

There were several statistically significant differences between the Eubacteria 16S rRNA treatment types. At the 24 hr time point, all of the iron treatments

decreased the bacterial population below that of the blank, negative control, and PvP-Ag NPs. There was no significant difference between the three iron treatments, and there was no significant difference between the blank, negative control, and PvP-Ag NPs. At the 72 hr time point, all iron samples decreased the population below that of the blank and negative control. The PvP-Ag NP treatment, however, was not statistically different from any of the other treatments. There was also no significant difference between the two iron nanoparticle samples, or between the blank and negative control. Finally, the bulk Fe treatment decreased the population below that of the bare nZVI treatment, but not that of the coated nZVI. Similarly, all iron samples decreased the population below that of the blank and negative control at the 168 hr time point. Additionally, the PvP-Ag NP treatment was not statistically different from any of the other treatments, and there was no difference between the iron nanoparticle samples. At this time point, however, the bulk Fe decreased the population below that of both iron nanoparticle treatments, and the negative control increased the population above that of the blank.

The results from the Archaea 16S ANOVA were similar to those of the Eubacteria 16S. At the 24 hr time point, the same trends were evident, except that the PvP-Ag NP treatment increased the microbial population above that of all other treatments. The same trends were also present at the 72 hr time point, but all iron samples had the same statistical effect of decreasing population. At the 168 hr time point, the findings were similar, except all iron samples had the same statistical effect, and the PvP-Ag NPs increased the population as compared with all other samples.

The dissimilatory sulfate reductase ANOVA did not produce many statistically significant results. The only significant difference at the 24 hr time point occurred between the PvP-Ag NPs and coated nZVI treatments. At the 72 hr time point, there were no significant differences between the treatments. Finally, the only differences at the 168 hr time point involved the PvP-Ag NPs. This treatment increased the sulfate reduction activity as compared with all iron treatments and the blank. Overall, the Eubacteria and Archaea 16S rRNA qPCR results revealed many statistically significant differences between the various experimental treatments. However, the significance of these differences in the dissimilatory sulfate reductase assay is limited.

Chapter 4: Discussion

4.1 Comparison of Nanoparticle Properties

The characterization techniques revealed many similarities between the two iron nanoparticle solutions. In terms of their stability in solution, the zeta potential measurements and TEM imaging both showed that the particles were moderately unstable and had a tendency to form loose aggregates. Furthermore, the individual particles in these aggregates had similar sizes (~5 nm difference) and specific surface areas (~1.1 m^2/g difference). In comparison, the PvP-coated silver nanoparticles appeared to be stable based on the zeta potential and low resolution TEM. However, high resolution imaging revealed that the 20-50 nm "particles" were actually tightly formed aggregates consisting of individual Ag particles with an average diameter of 4 nm and specific surface area of 143 m^2/g. This finding matches descriptions in other papers and could mean an increased surface reactivity for the PVP-Ag NPs.[79]

In terms of their surface chemistry, the bare and coated nZVI mainly consisted of iron surrounded by a carbon, oxygen, and hydrogen protective layer. The total percentages for each element were nearly identical between the two samples. The high-resolution spectra, however, revealed some important differences in composition. The coated nZVI contained a much higher percentage of COOH and O^{2-} than the bare particles, which mainly consisted of C-C/C-H and organic O. These differences may be related to the stabilization agents used during production and shipment of the nanoparticles: the different C 1s compositions could be explained by

structural dissimilarities between the organic stabilizers of the two samples, and the increased O^{2-} could be from oxygen bonds in the un-described inorganic modifier (i.e. SiO_2 or Al_2O_3) on the coated nZVI. The increased O^{2-} could also result from greater iron oxidation of the coated nZVI. This is unlikely, however, because the iron percentages and high-resolution spectra are almost identical between the two samples. In both cases, the iron high-resolution spectra best correlated with iron oxide (most likely FeO), with no metallic iron in the coated nZVI sample and only minimal amounts in the bare nZVI. This characteristic did not change significantly throughout the ion sputtering analysis, although the total iron percentage did increase with depth.

Conversely, the PvP-Ag nanoparticles were solely metallic in nature, with no evidence of oxidation. This is a significant difference between the iron and silver nanoparticle samples, which likely impacts the surface reactivity in solution. Iron oxide is known to inhibit reactions involving nZVI, although most studies refer to Fe_2O_3, rather than FeO.[80] FeO can still react with materials through the oxidation of Fe^{2+} ions. Additionally, the cores of the nanoparticles are likely protected from oxidation and may remain in the zero valence state. Therefore, the iron nanoparticle solutions could exhibit significant reactivity despite surface oxidation. Furthermore, the iron oxidation on the surface may be a result of the drying process and subsequent exposure to air, rather than an inherent failure of the surface modifiers. It is possible that the protective surface coatings are more effective in solution due to an increased reducing atmosphere.

4.2 Relationship between Water Chemistry and Microbial Ecology

Each of the iron treatments produced a pH increase and ORP decrease when compared with the other experimental samples. These treatments also resulted in significantly lower microbial populations, as measured by the Eubacteria and Archaea 16S rRNA qPCR assays. Interestingly, these changes in chemistry and microbial ecology followed similar trends: observed changes occurred within 24 hours after treatment, they stabilized and persisted for the entirety of the experiment, and they were very similar between the different iron treatments. Therefore, there may be a connection between the observed pH and/or ORP and the measured microbial populations.

With regards to pH, the increases from the iron treatments resulted in neutral-slightly alkaline media. Because many anaerobic microbes (i.e. methanogens and sulfate reducers) have an optimum pH range of 7.5-8.5, this increase is unlikely to cause substantial damage and may even increase metabolic rates.[81] Additionally, anaerobic microbes are typically more resistant to stressors than aerobic microorganisms, so a change of 1-1.5 pH units should not significantly impair their growth or viability.[82] Furthermore, the negative control and silver nanoparticle treatments resulted in similar pH values as the iron-treated samples. These treatments, however, did not cause significant microbial death and instead increased the population at some time points. Therefore, the higher pH of the iron samples may be a result, rather than a source, of the microbial response. This is supported by the observation that microbial growth can decrease solution pH.[83] Consequently, the

iron-treated samples may have the highest pH values, because they possess the smallest population of microbes capable of releasing hydrogen ions through growth.

Regarding the oxidation-reduction potentials, the observed decreases in the iron samples can be explained by redox chemistry. When zero-valent iron and FeO enter the system, Fe(0) and Fe(II) have the potential to be oxidized to Fe^{2+} and/or Fe^{3+} ions. Therefore, the iron creates a reducing environment, which is characterized by a negative ORP value. This decrease in the reduction potential may be sufficient to explain the observed microbial death. Microorganisms are sensitive to chemical changes in their environment, and certain types of metabolic processes can only occur under specific redox conditions.[84,85] Therefore, changes in ORP can interrupt cellular respiration and decrease the microbial population. The observed microbial death could also result from iron oxidation via reduction of another material (i.e. TCE). This redox reaction would release iron ions into solution, where they may generate reactive oxygen species via the Fenton reaction. These species can then disrupt the cellular membranes of microorganisms via lipid peroxidation, resulting in cell lysis and death.[31,54]

It is also possible that the observed changes in ORP are a result of microbial activity. Microorganisms can impact the reduction potential of a system through respiration and growth.[86] Therefore, the positive ORP values in the blank, negative control and PVP-Ag NP samples may be from their greater microbial populations. Conversely, the ORP values of the iron treatments could be a consequence of the microbial death in these samples. While this interaction may have occurred to an extent, it is unlikely the primary source of the drastic decreases in ORP. A relatively

large concentration of iron was added to each of these samples, so a significant drop in the systems' redox potentials should be observed. If there is any correlation between ORP and population, it is more plausible that microbial death resulted from the reducing environment and/or the release of iron ions.

4.3 Impact of Experimental Treatment

The methanogenesis activity and *Dehalococcoides* spp. population were below the detection limits of the qPCR methyl coenzyme M reductase and 16S rRNA assays, respectively. Treatment impacts involving these two microbial groups could therefore not be measured in this experiment. Additionally, the sulfate reduction activity in most samples was only slightly greater than the detection limit of the dissimilatory sulfate reduction assay. Consequently, it was difficult to discern any significant trends in the data, and the ANOVA analyses revealed limited or no statistical differences between the various treatment types.

The Bacterial and Archaeal 16S rRNA assays, however, revealed many significant differences between the total Bacteria and Archaea populations in the different experimental samples. Regarding the samples treated with the negative control, there was no statistically significant impact at either the 24 or 72 hr time points, as compared with the blank. At the 168 hr time point, however, this treatment significantly increased the bacterial population, but decreased the archaeal one. The reason for this differing effect is unknown, but it is possible that the pH increase or ethanol addition stimulated bacterial activity while hindering archaeal growth due to differences in the microbial metabolisms. It can be concluded that the negative

control (pH 10, 4.2% ethanol DI water) generally did not interact significantly with the microorganisms in the groundwater samples, and when an interaction did occur, the impact was limited and inconsistent between the different microbes.

The silver nanoparticles were originally designed as a positive control due to their demonstrated toxicity to a wide array of microorganisms (including some anaerobic species).[87-90] The qPCR results, however, revealed a trend of increasing bacterial and archaeal GCNs over time when treated with the PvP-Ag NPs. In all cases, the average microbial populations in the silver nanoparticle-treated samples were distinctly greater than those of all other samples. Although these increases were only statistically significant in two cases (Archaea 16S rRNA at t=24 and t=72), it was evident that the PvP-Ag NPs were not toxic to the microbes. This is especially surprising considering the extremely large dose of spiking solution used in this experiment (the final concentration was approximately 100 times greater than that of most other studies).[45,88-91] These results agree with a few recent studies that have found silver nanoparticles are not toxic in anaerobic environments.[92,93] Researchers hypothesize that the absence of oxygen prevents silver ions from being released into solution.[94,95] Therefore, there does not appear to be a unique nanoparticle-based toxicity in this or other studies. Instead, silver ions appear to be responsible for microbial death.

Finally, analysis of the iron-treated samples revealed that all experimental treatments decreased the bacterial and archaeal populations below that of the blank and negative control. These findings were significant at the 90% confidence level and indicate an apparent microbial toxicity that is uniquely iron-based, rather than pH

or ethanol-related. Furthermore, the three treatment types (bulk Fe, bare iron nanoparticles, and coated iron nanoparticles) had comparable impacts on the microbial communities. There were only statistically significant differences between these treatments in two cases: Eubacteria 16S rRNA assay at the t=72 and t=168 hr time points, where the bulk Fe treatment decreased the bacterial population below that of one or both of the nanoparticle treatments. From these results, there does not appear to be a unique nanoparticle-based toxicity. Instead, the toxicity seems to result either from the release of iron ions and production of reactive oxygen species, or from the drop in redox potential and disruption of microbial metabolisms.

Chapter 5: Conclusion

5.1 Significance

This study produced some interesting findings that could have implications for future nanoparticle applications. Surprisingly, the silver nanoparticles in this study did not exhibit any microbial toxicity. The PvP-Ag actually increased the bacteria and archaea populations in the anaerobic system. This finding supports the theory that Ag^{+} ions are the source of silver toxicity, rather than a unique nanoparticle-based effect. Therefore, silver nanoparticles cannot be used as bactericidal agents in anaerobic systems. nZVI, however, may be an advantageous replacement.

Both bare and coated nZVI were toxic to the anaerobic groundwater microbes in this study. This toxicity was equivalent to that of iron filings when applied in equal concentrations. Consequently, the toxic effect was likely a result of iron ion release or redox shifts, rather than a unique nanoparticle-based toxicity. This conclusion is supported by other studies, but there is still some controversy over the mechanism of toxic action. Regardless of the cause, nZVI exhibits bactericidal properties in anaerobic environments, making it useful for a wide array of industrial applications in addition to its current uses in environmental remediation. These particles, for example, could be used in disinfectants for the removal of microbial pathogens, or in wastewater treatment plants for the prevention of microbial build-up on filtration membranes.

5.2 Future Work

The findings presented in this study suggest the microbial toxicity of both bulk and nano zero-valent iron. However, the precise mechanism of this toxicity could not be determined. Other studies are needed to discern the source of toxicity and confirm the absence of a unique nanoparticle effect. Inoculation of microbes with ferrous and ferric salts could determine if iron ions are responsible for the observed toxicity. Oxidant scavengers could also be added to the experiment to see if reactive oxygen species are required for cellular death. Furthermore, measuring microbial death at varying Fe concentrations and ORP values could allow for a statistical comparison of correlation. Using this approach, it could be possible to determine which factor has a greater impact on toxicity.

This study raises some important questions involving the use of zero-valent iron for contaminant removal. The results suggest that iron filings, bare nZVI, and coated nZVI are toxic to anaerobic microorganisms. Therefore, the use of these materials for the remediation of groundwater could cause noticeable damage to the native microbial communities. More studies are needed to investigate the extent and permanence of this damage in natural settings. A field study involving the addition of ZVI to contaminated groundwater that measures both the TCE concentration and microbial populations over an extended period of time would provide valuable information for a cost-benefit analysis of this remediation technique. As the current research stands, there are still many uncertainties surrounding zero-valent iron nanoparticles in the environment, but there is clear evidence of toxicological action that could be of ecological concern.

Appendices

Appendix A: Experimental Diagram

The experiment consisted of four basic components:
the enrichment culture preparation (green), the nanoparticle preparation and characterization (yellow), the toxicity study (purple), and the qPCR analysis (blue).

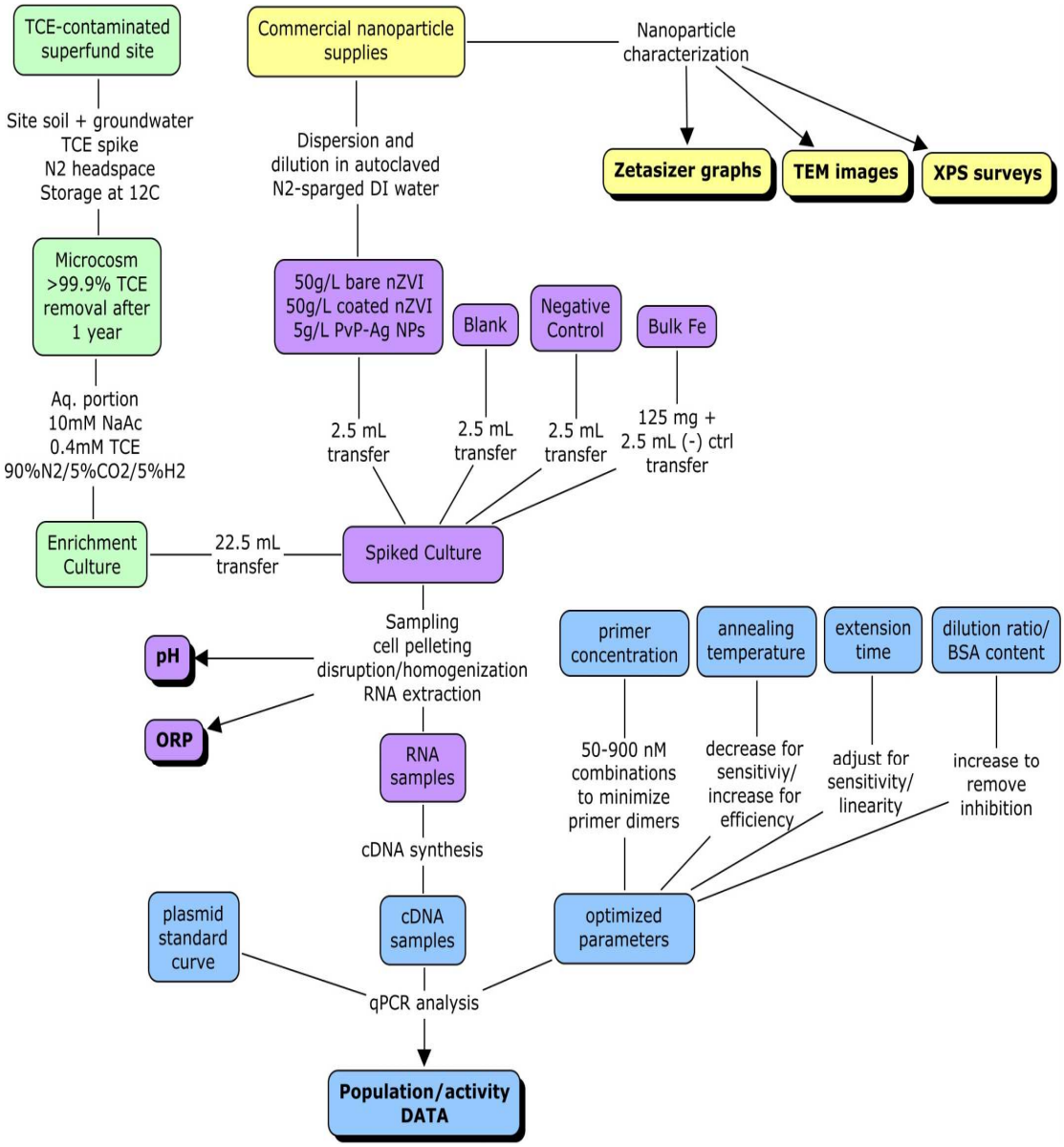

Appendix B: Gene Copy Number Calculation

GCN = (g DNA * Avogadro's number) / (base pairs of the gene * avg. mass of DNA)

GCN = (g DNA * 6.02E23) / [(3956 + base pairs of the insert)* 660]

Appendix C: Optimum qPCR Conditions

Assay	**Primer Concentration, forward:reverse (nM)**	**Annealing Step, temperature – time**	**Extension Step, temperature – time**
Eubacteria 16S	300:50	57°C – 30s	60°C – 30s
Archaea 16S	300:900	57°C – 30s	60°C – 30s
Dissimilatory sulfate reductase	900:300	55°C – 30s	60°C – 60s

Appendix D: XPS Surveys

PvP-Ag NPs: High-Resolution Survey

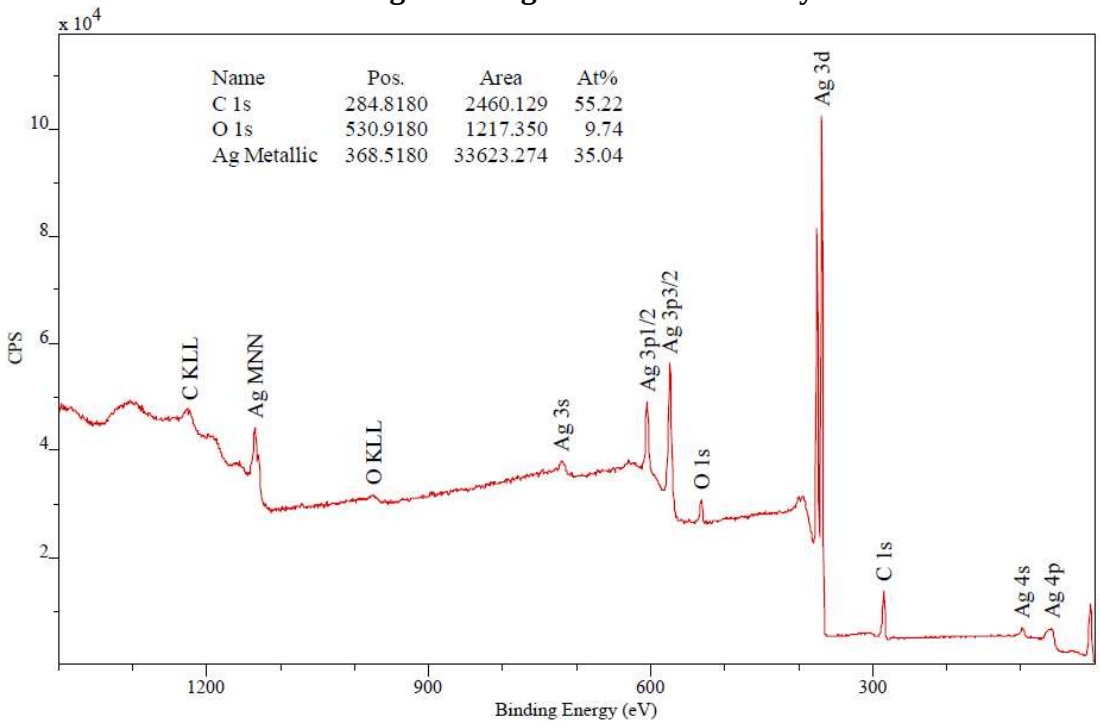

PvP-Ag NPs: C 1s

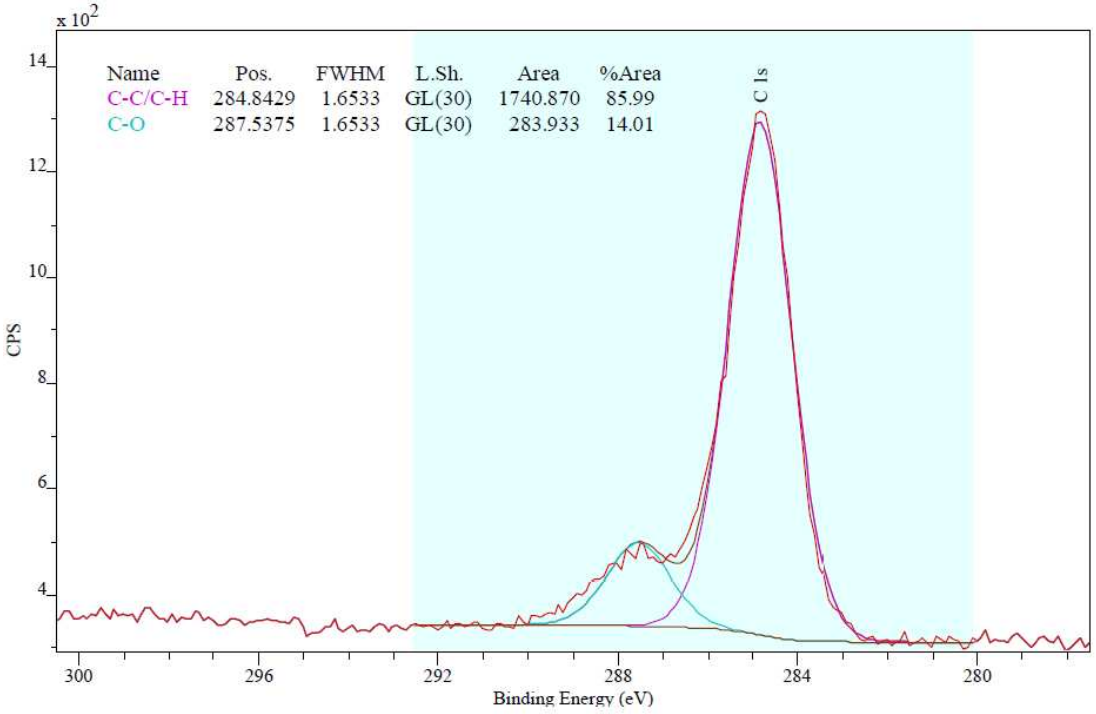

PvP-Ag NPs: O 1s

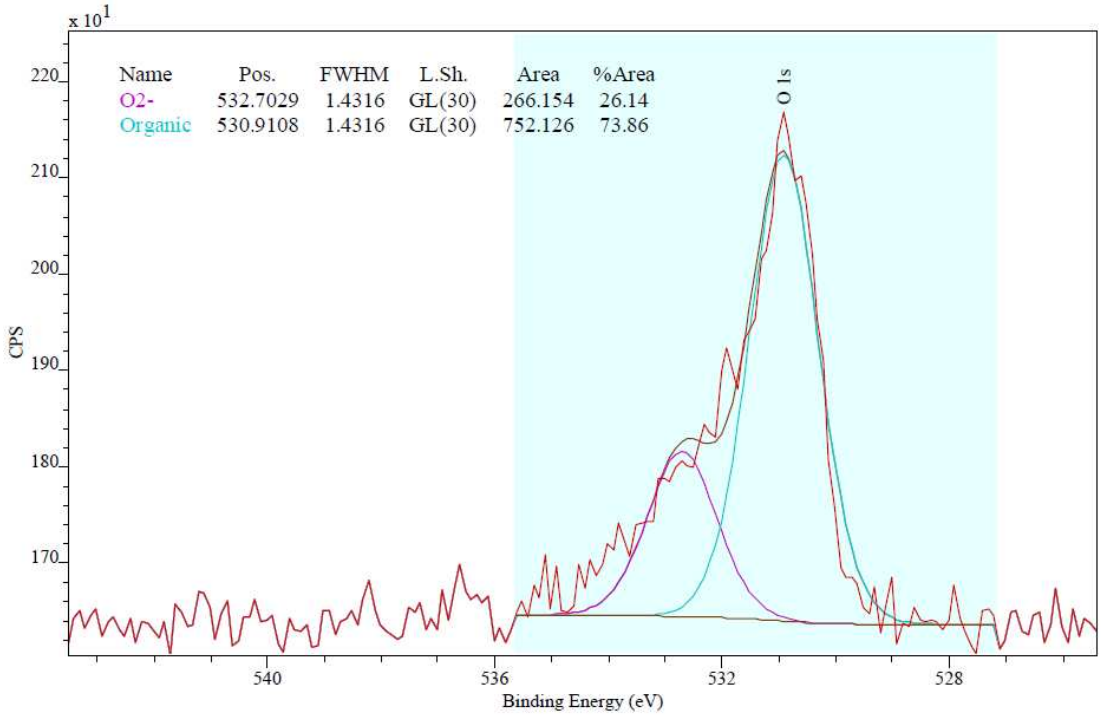

PvP-Ag NPs: Ag 3d

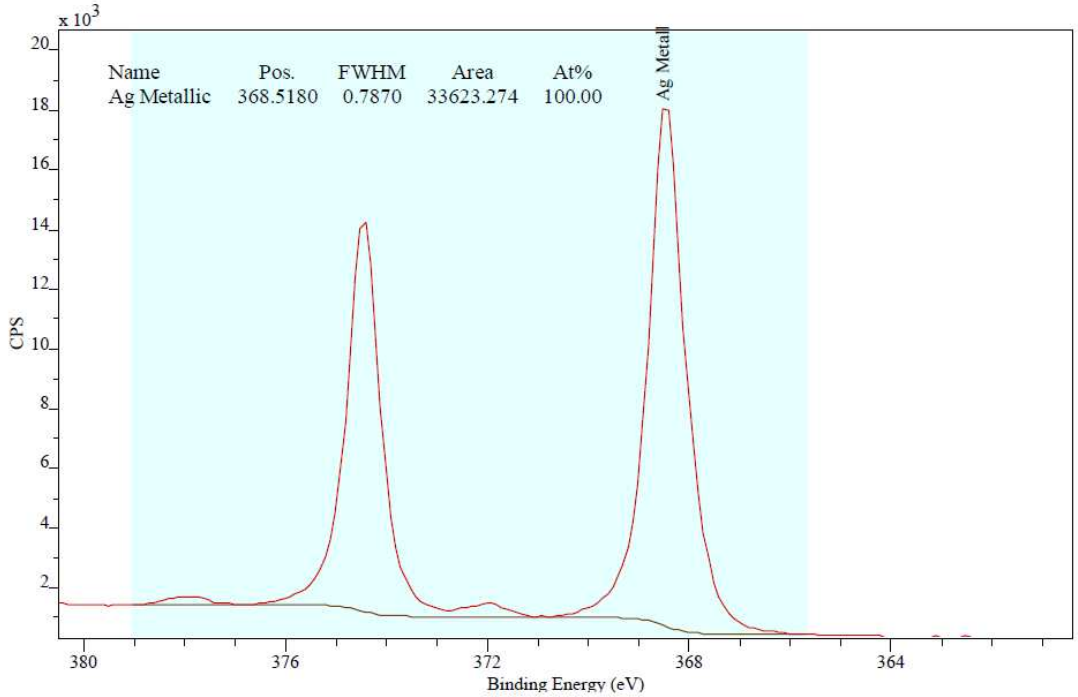

Bare nZVI: High-Resolution Survey

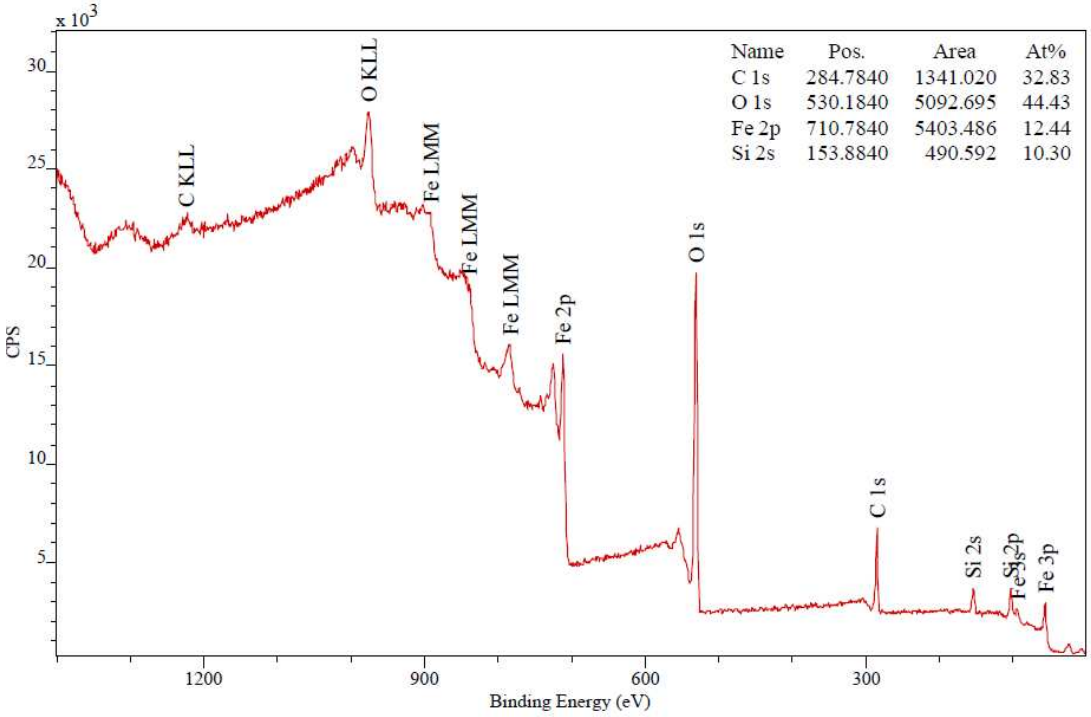

Bare nZVI: C 1s

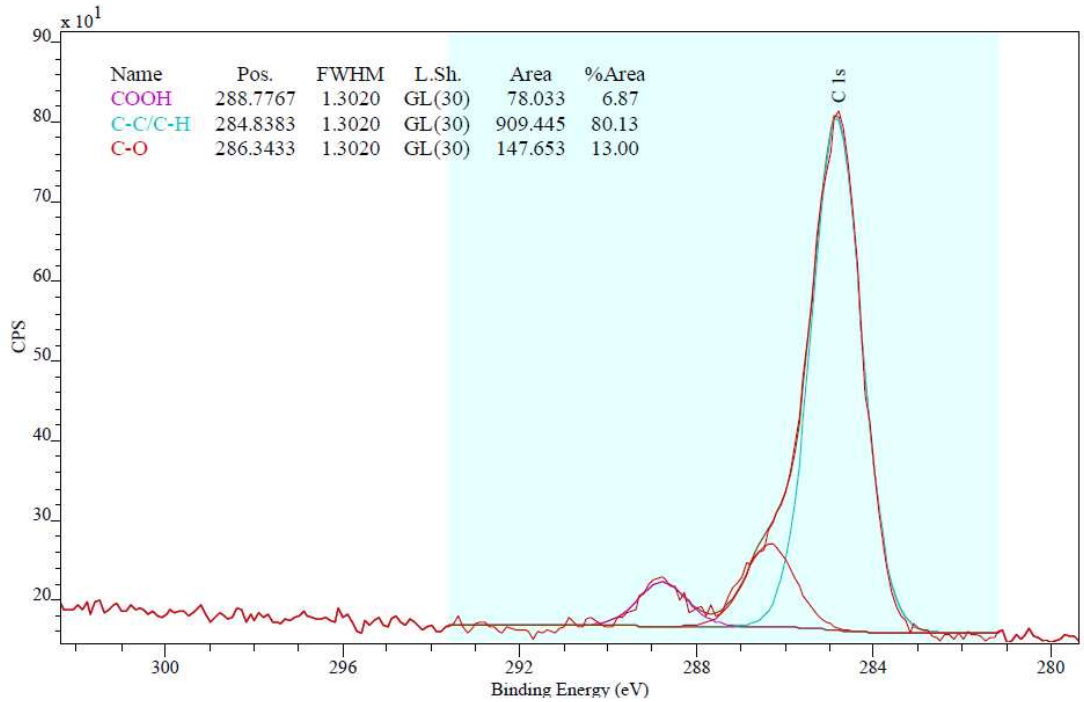

Bare nZVI: O 1s

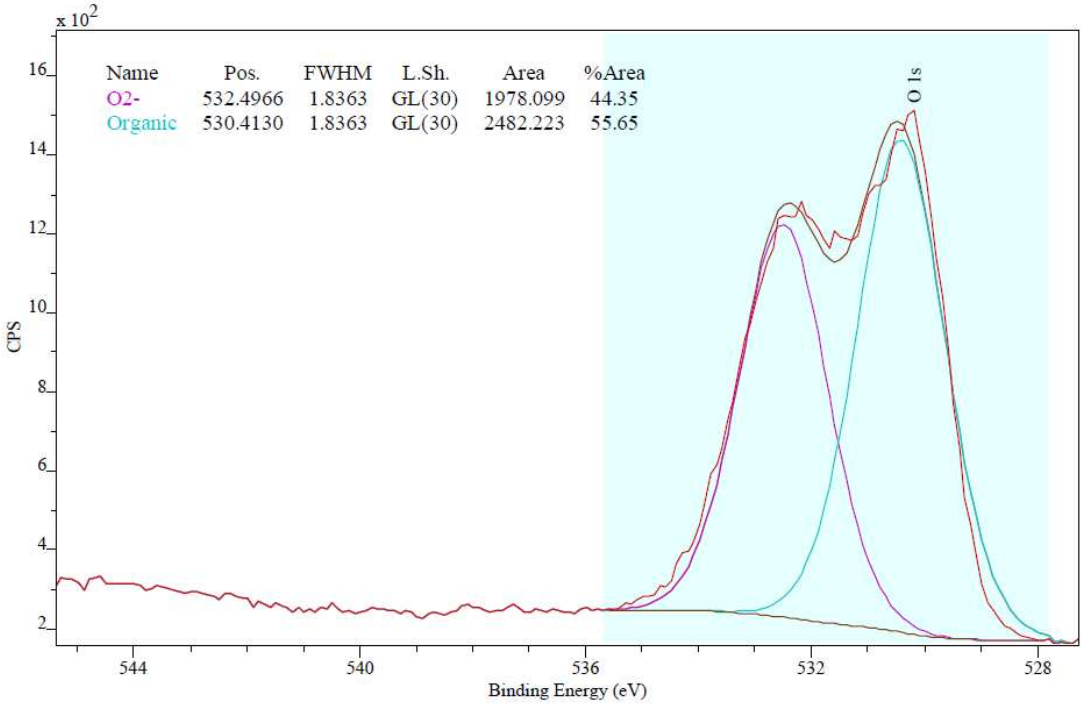

Bare nZVI: Fe 2p

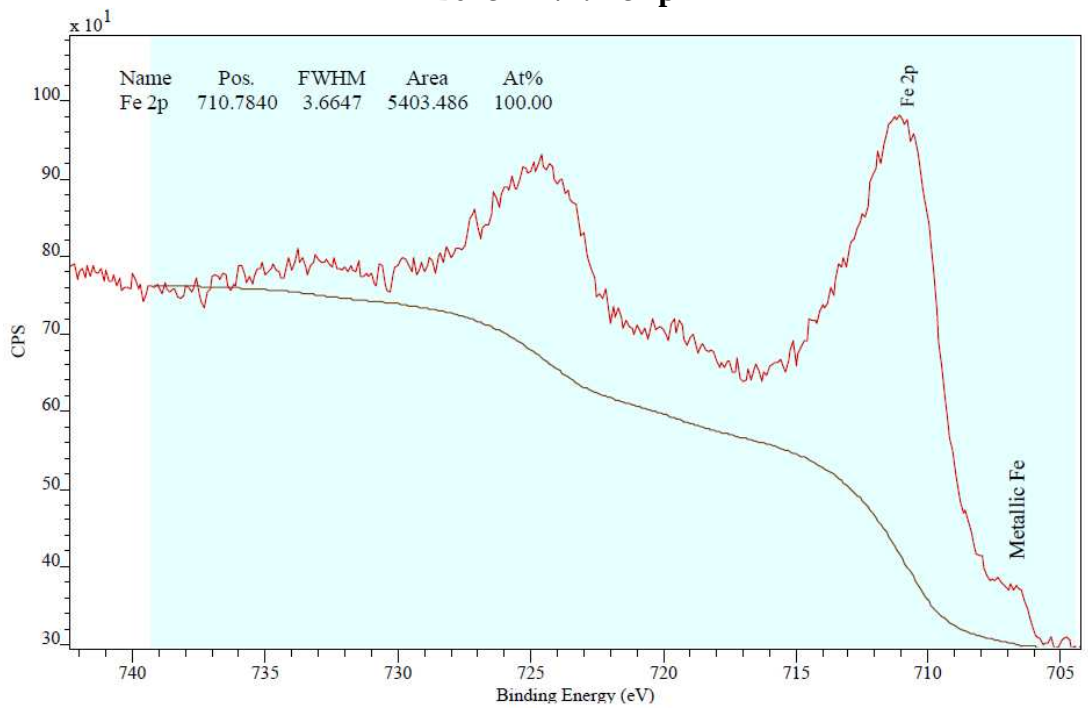

Coated nZVI: High-Resolution Survey

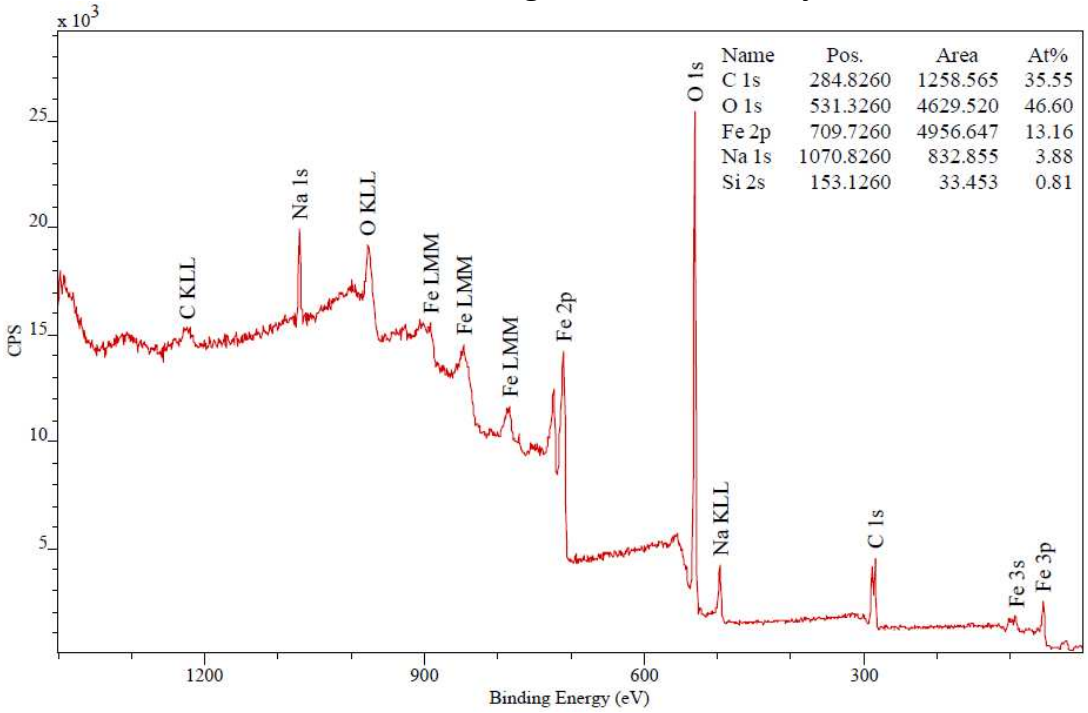

Coated nZVI: C 1s

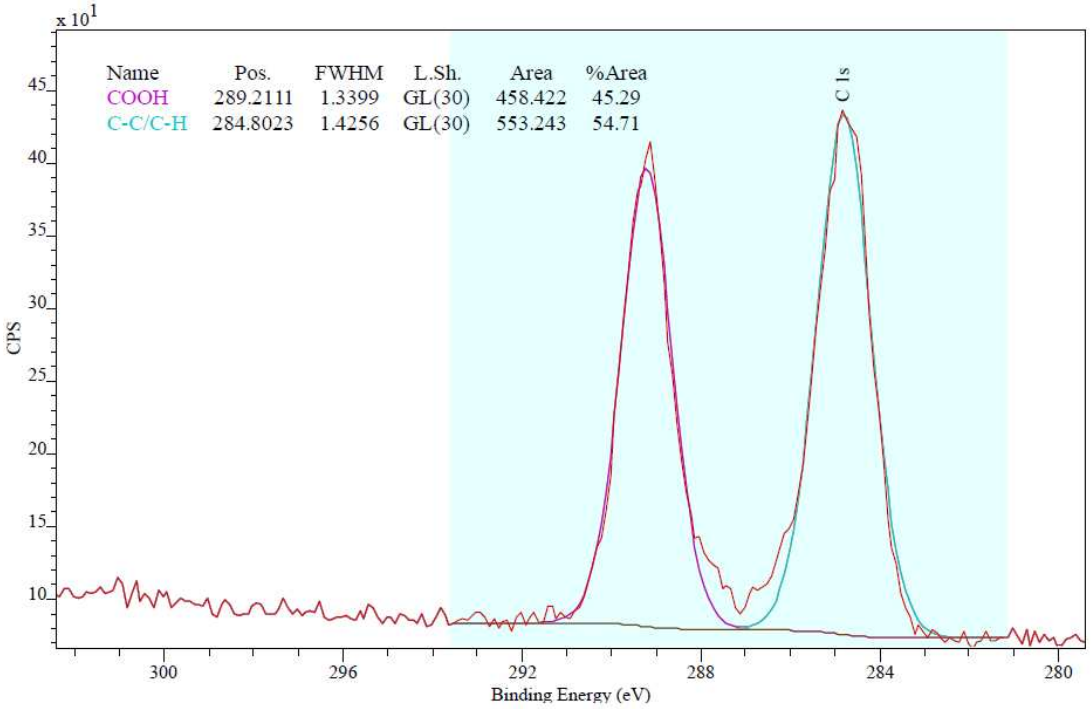

Coated nZVI: O 1s

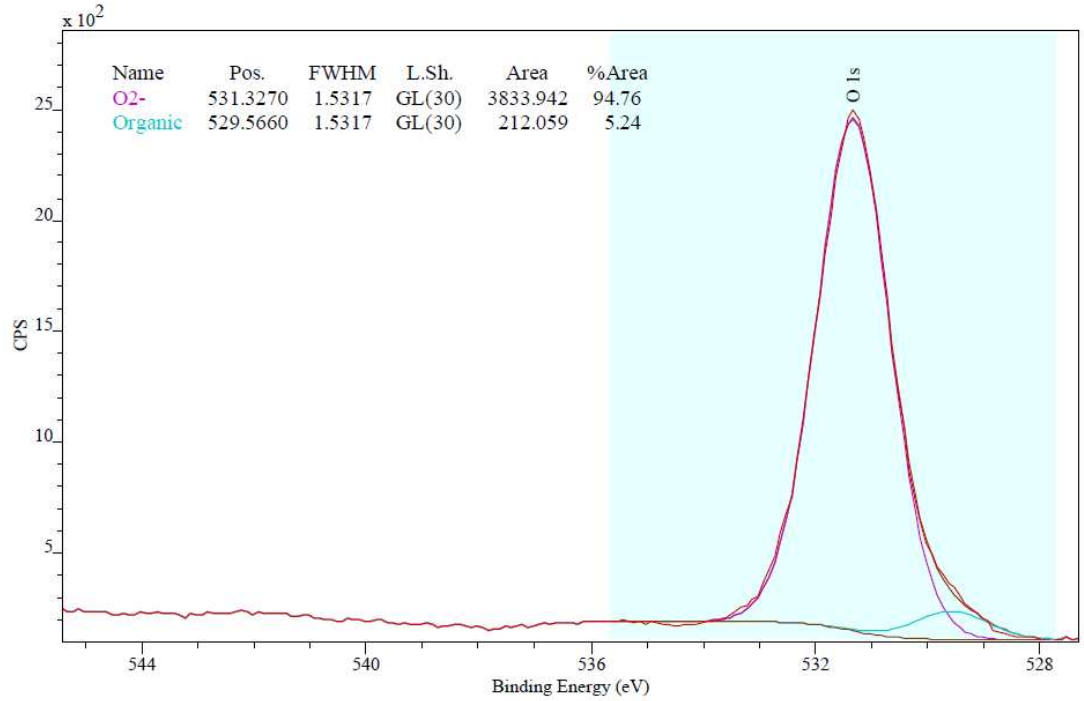

Coated nZVI: Fe 2p

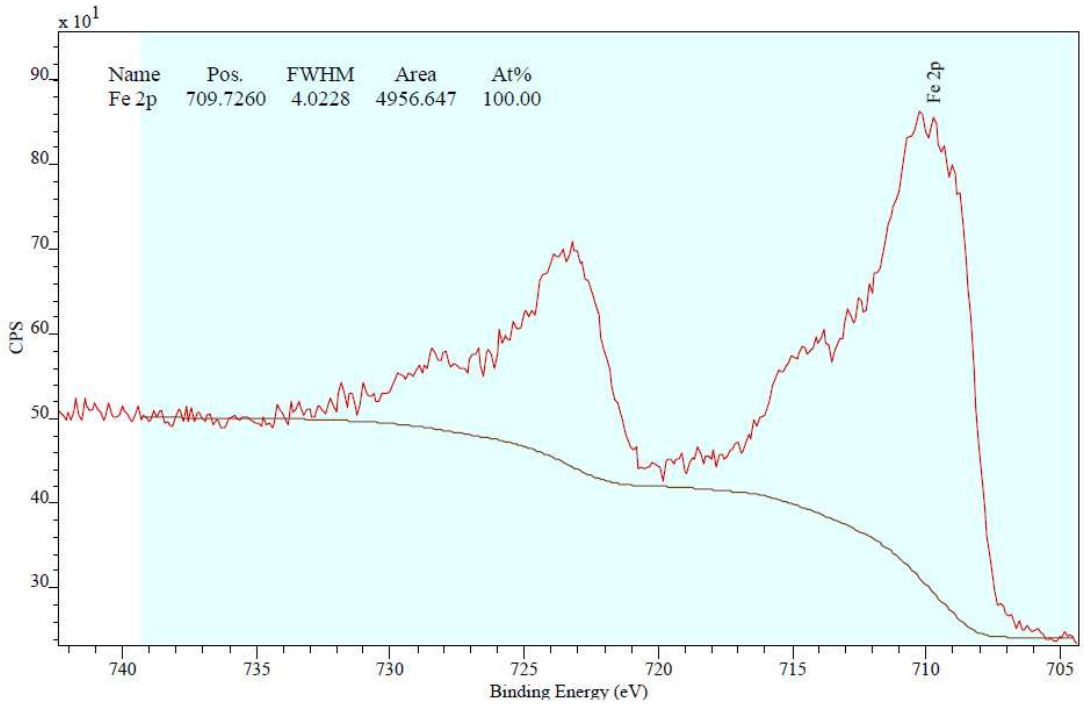

Appendix E: XPS Depth Profiles

Bare nZVI Ion Sputter 4: High-Resolution Survey

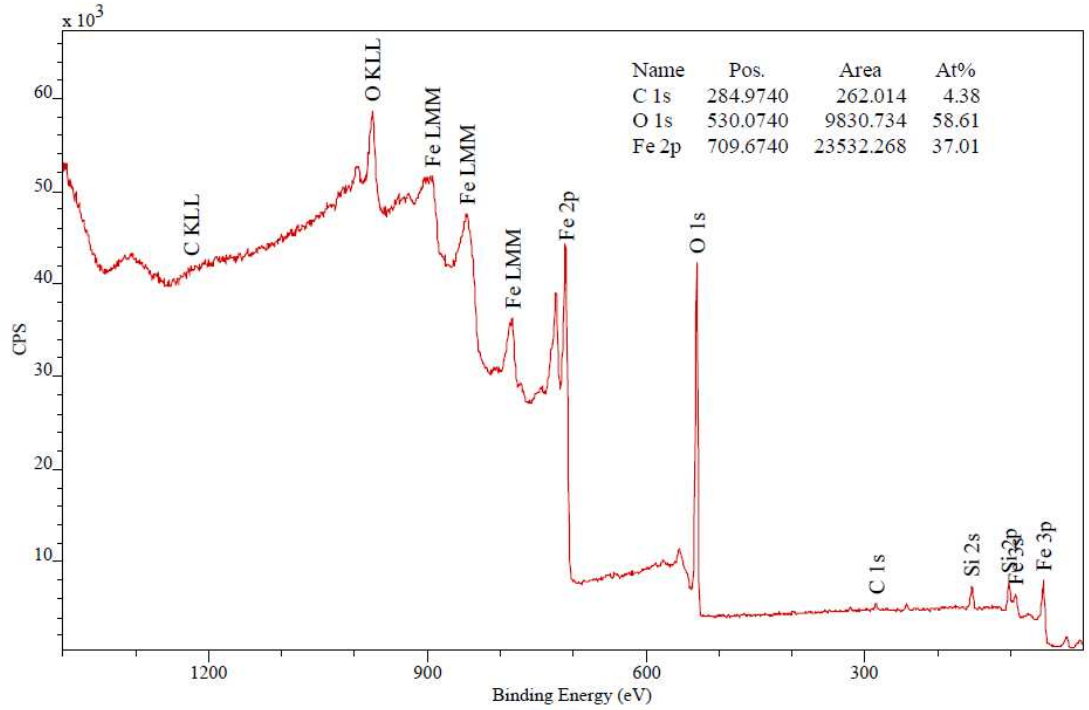

Bare nZVI Ion Sputter 4: C 1s

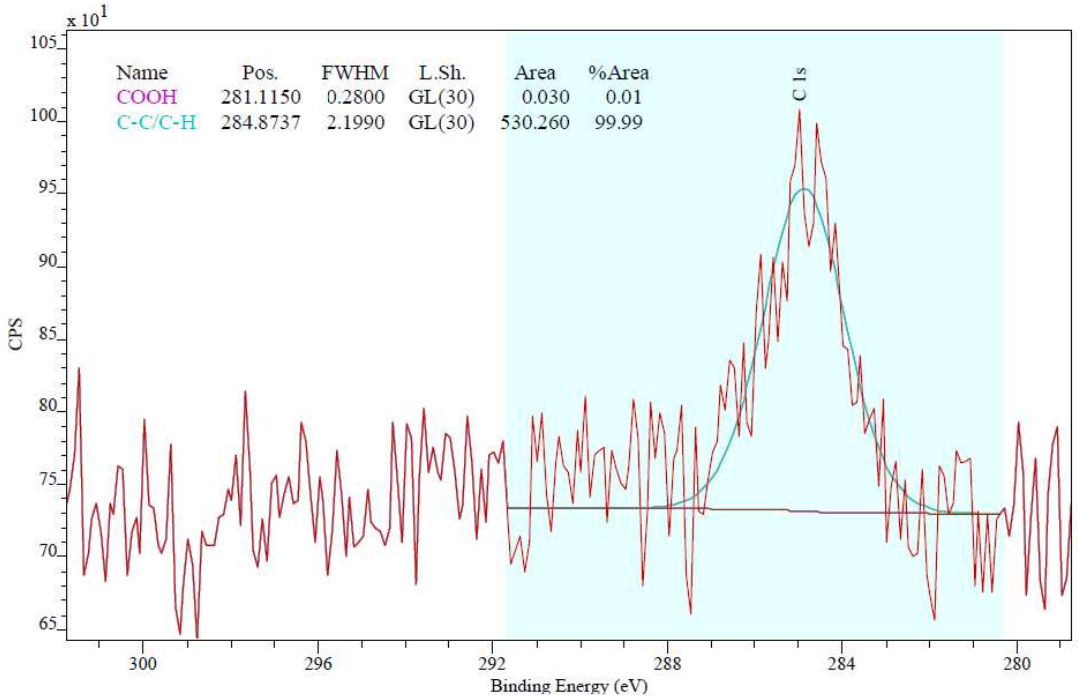

Bare nZVI Ion Sputter 4: O 1s

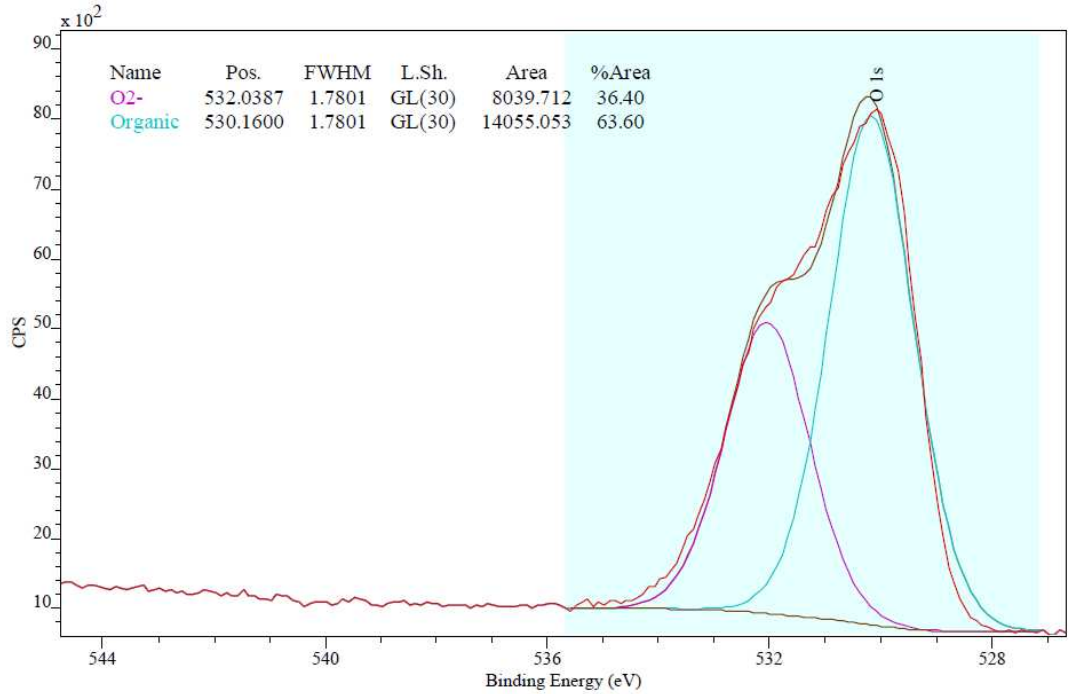

Bare nZVI Ion Sputter 4: Fe 2p

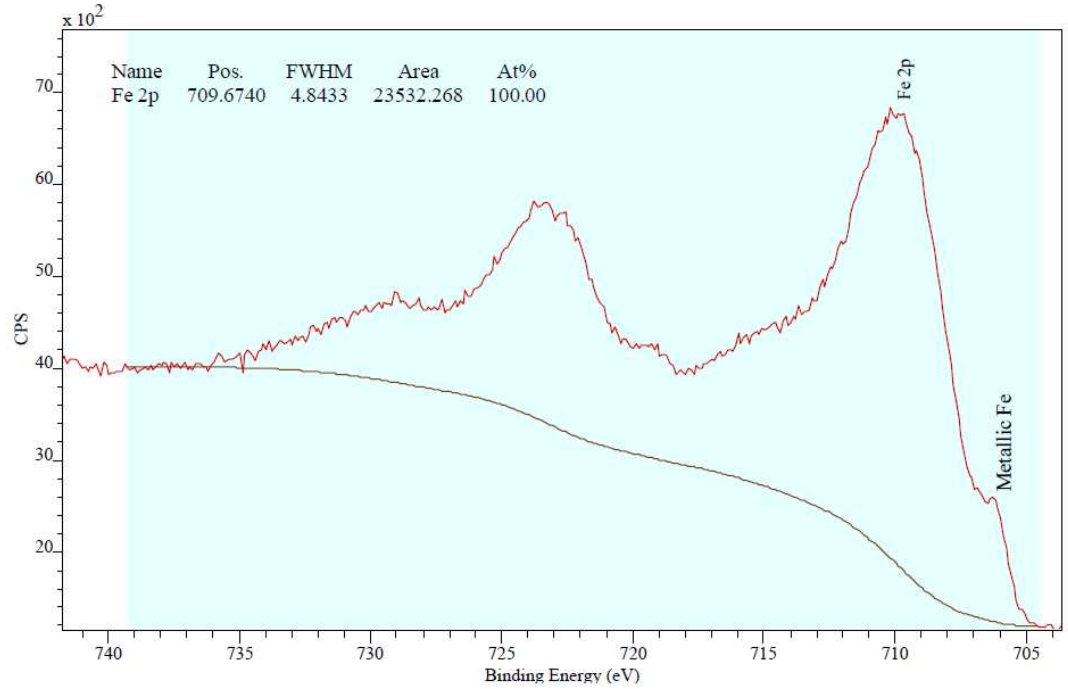

Coated nZVI Ion Sputter 4: High-Resolution Survey

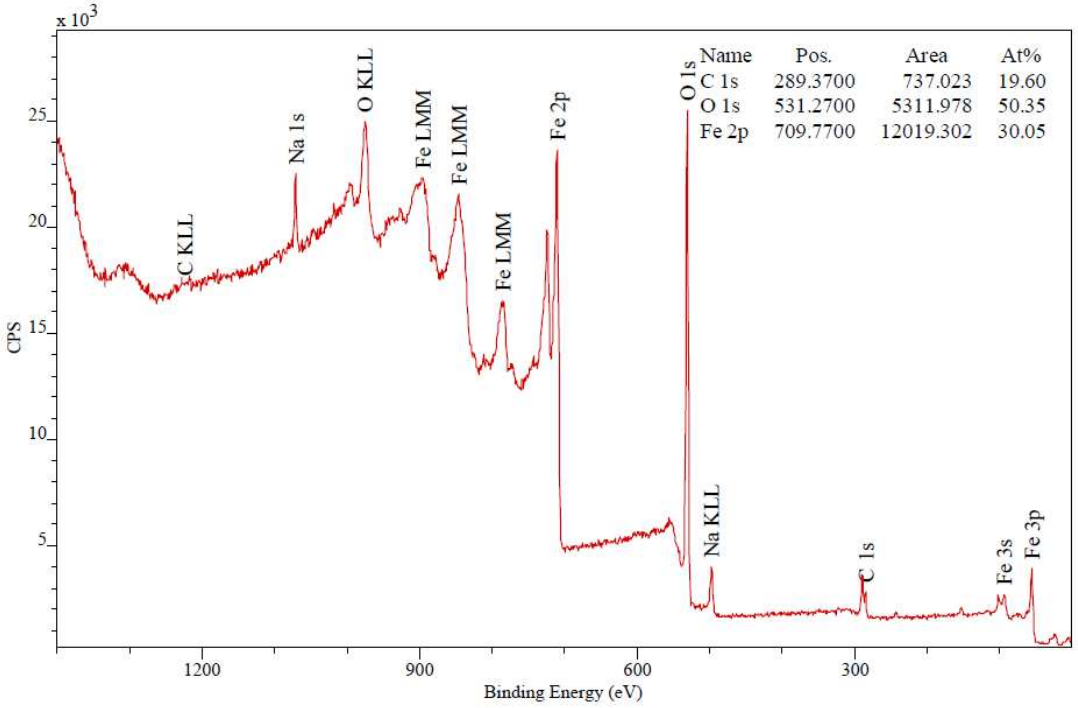

Coated nZVI Ion Sputter 4: C 1s

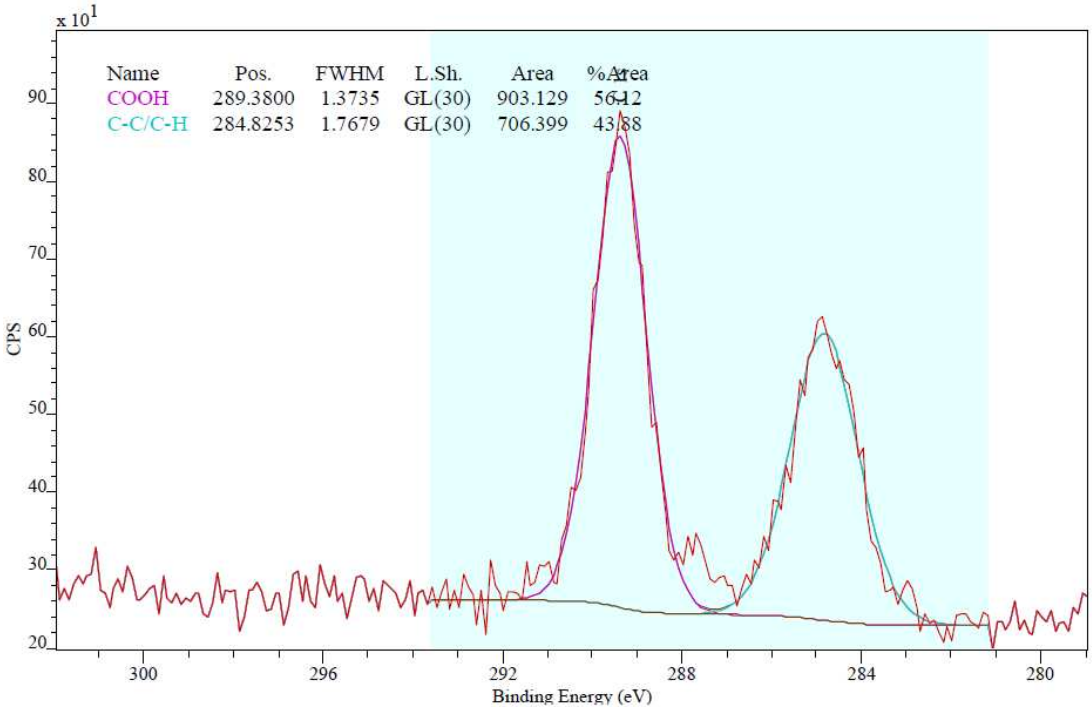

Coated nZVI Ion Sputter 4: O 1s

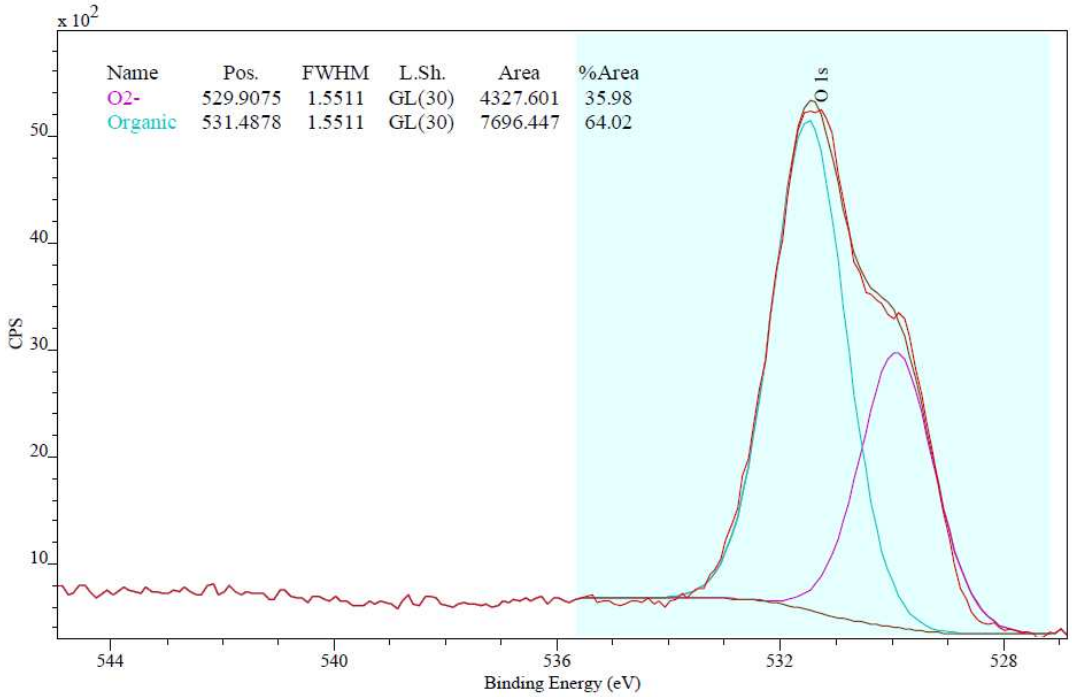

Coated nZVI Ion Sputter 4: Fe 2p

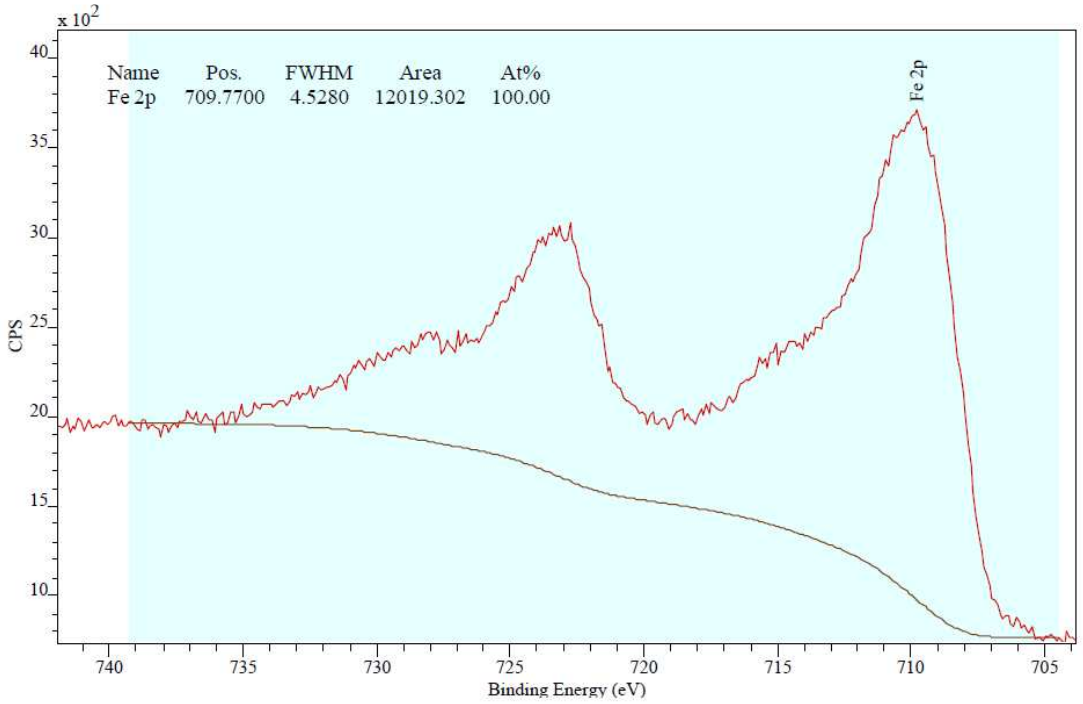

Appendix F: Sample Concentration Calculation

Gene copies/mL culture = GCN / volume qPCR sample * dilution factors * extraction volume / sample volume

Gene copies/mL culture = GCN / 2 µL * (40/3) * 50 µL / 5 mL

Appendix G: Welch ANOVA Results

Mean plots from the Welch ANOVA analysis using Games-Howell post-hoc tests are presented in the following format:

a) The number on the x-axis refers to the type of spiking solution used in the toxicity study: 1=blank, 2=negative control, 3=PvP-Ag NPs, 4=bulk Fe, 5=bare nZVI, and 6=coated nZVI

b) The y-axis corresponds to the mean gene copy number of the experimental replicates for the Eubacteria 16S, Archaea 16S, or dissimilatory sulfate reductase qPCR assay at the T=24, 72, or 168 hr time point

c) Any number above a data point on the plot corresponds to a treatment type that is statistically different at the 90% confidence level (i.e. a number 4 above the spike 1 data point indicates that there is a statistically significant difference between the means of the bulk Fe and blank treatments)

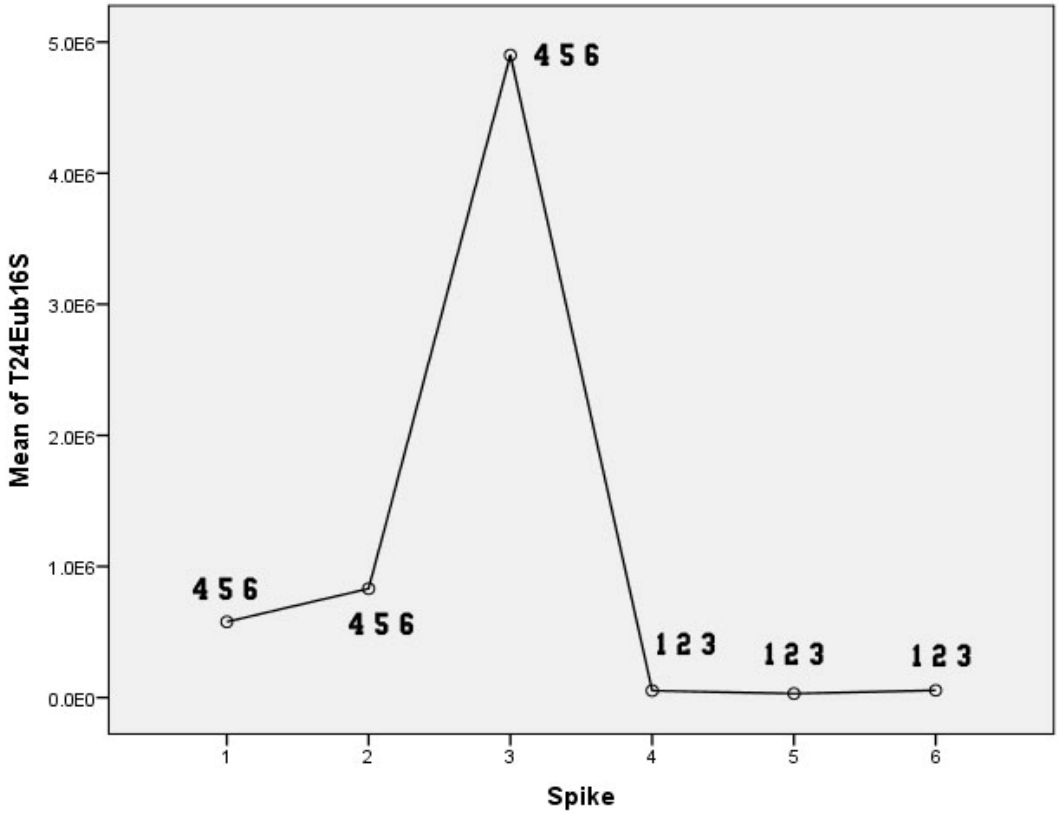

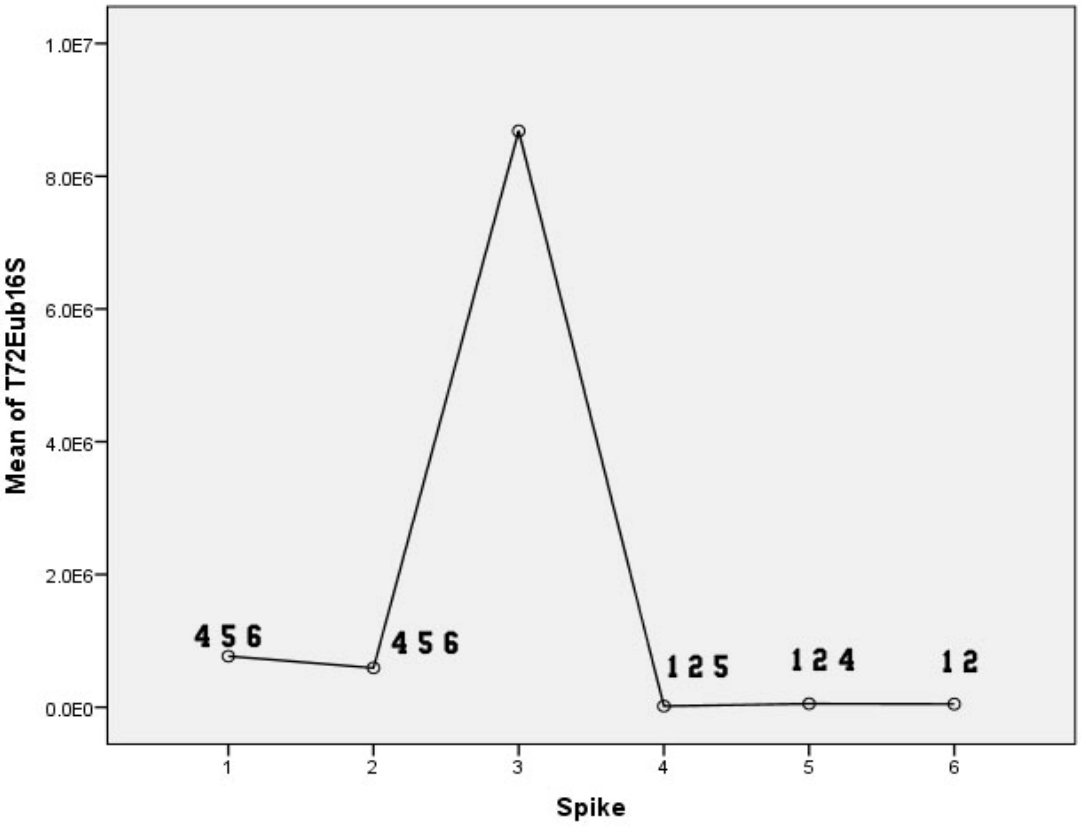
Mean of T72Eub16S
1.0E7
8.0E6
6.0E6
4.0E6
2.0E6
0.0E0
4 5 6
4 5 6
1 2 5
1 2 4
1 2
1
2
3
4
5
6
Spike

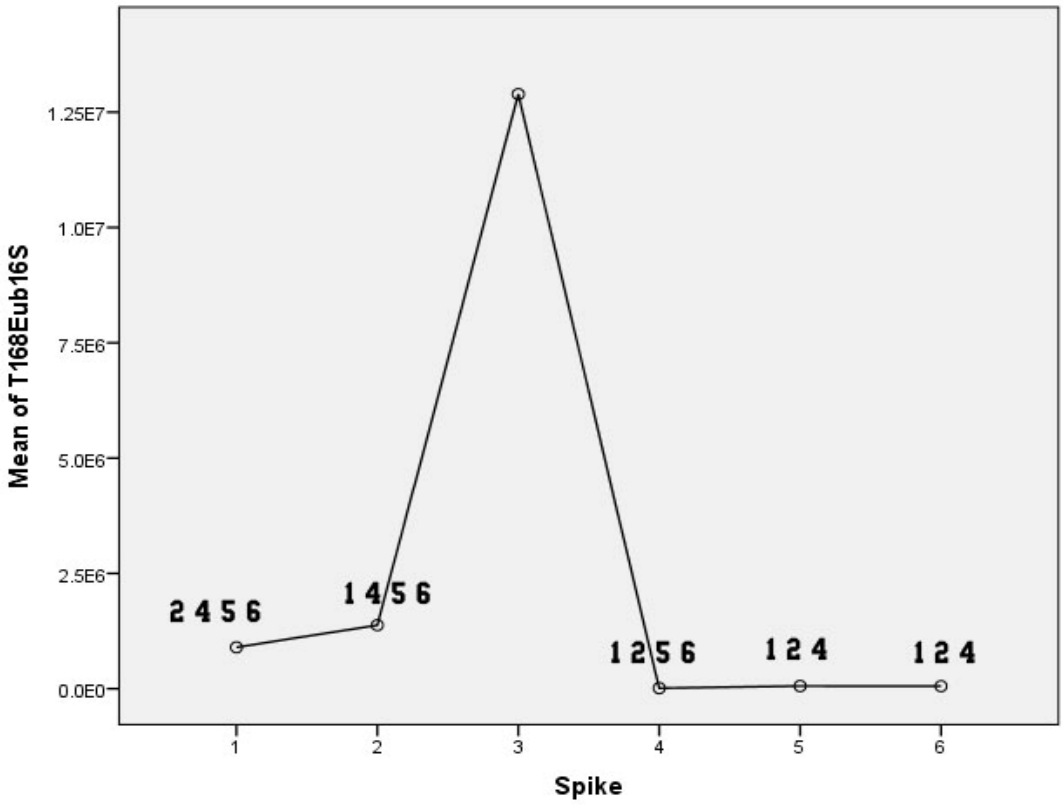
Mean of T168Eub16S
1.25E7
1.0E7
7.5E6
5.0E6
2.5E6
0.0E0
2 4 5 6
1 4 5 6
1 2 5 6
1 2 4
1 2 4
1
2
3
4
5
6
Spike

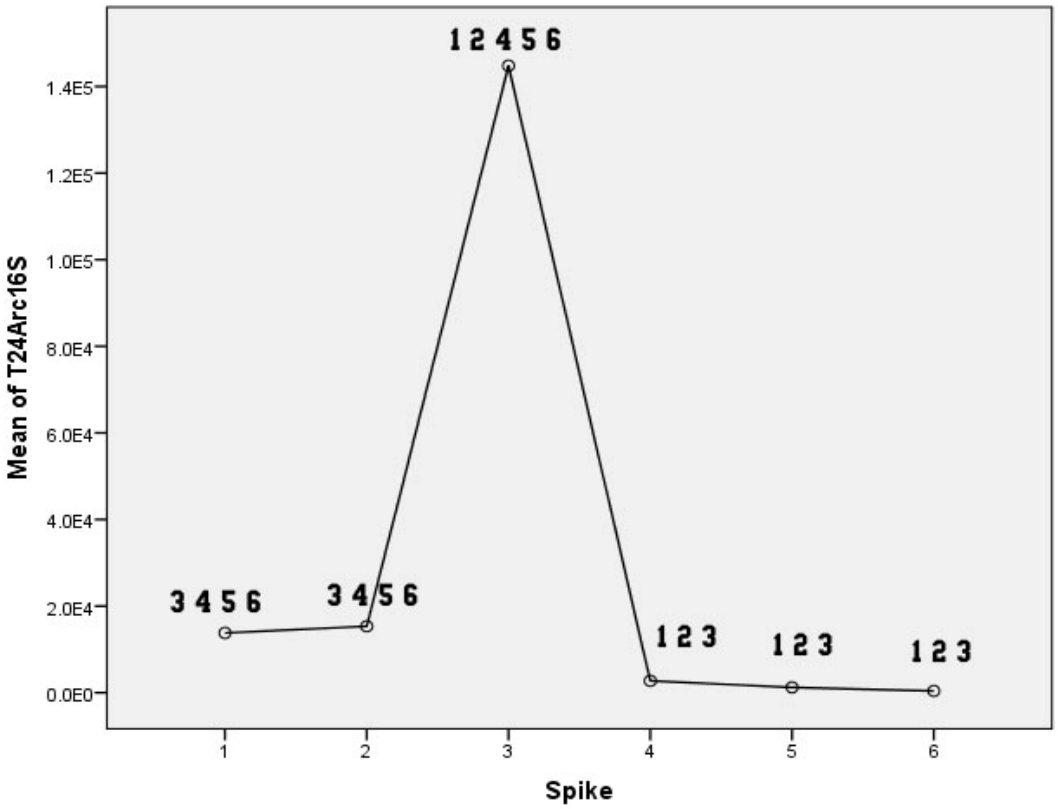
Mean of T24Arc16S
1.4E5
1.2E5
1.0E5
8.0E4
6.0E4
4.0E4
2.0E4
0.0E0
1 2 4 5 6
3 4 5 6
3 4 5 6
1 2 3
1 2 3
1 2 3
1
2
3
4
5
6
Spike

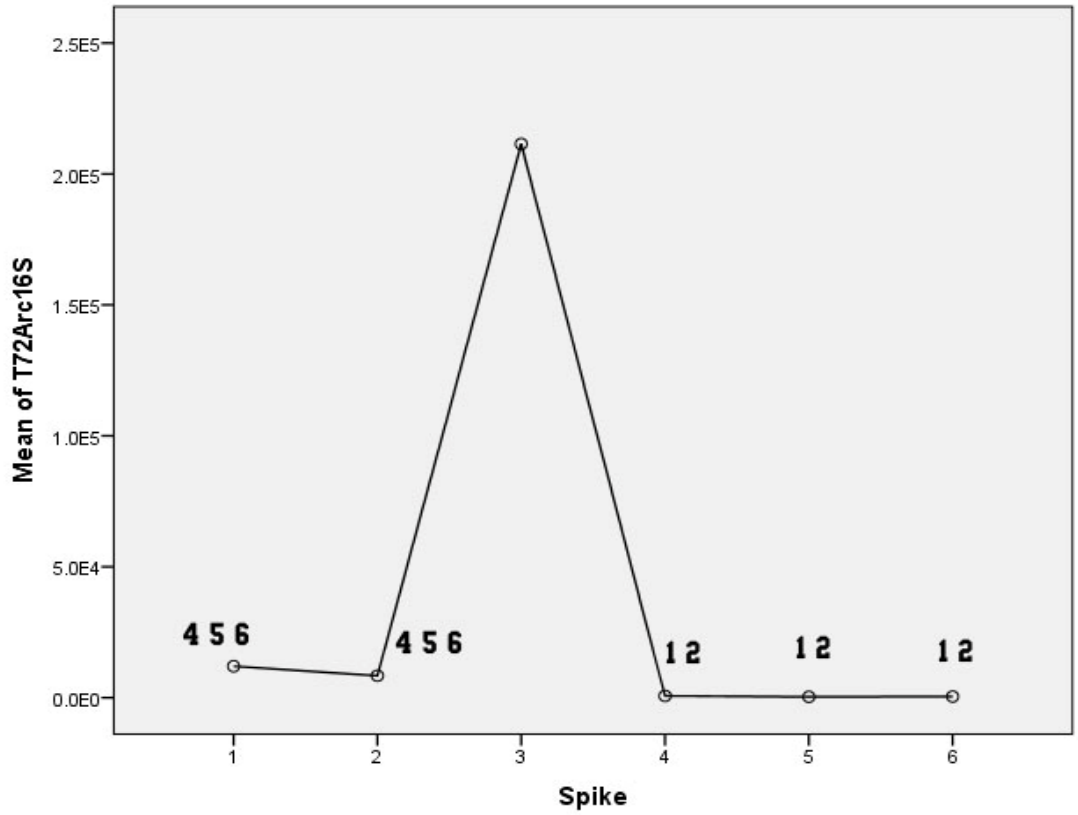
Mean of T72Arc16S
2.5E5
2.0E5
1.5E5
1.0E5
5.0E4
0.0E0
4 5 6
4 5 6
1 2
1 2
1 2
1
2
3
4
5
6
Spike

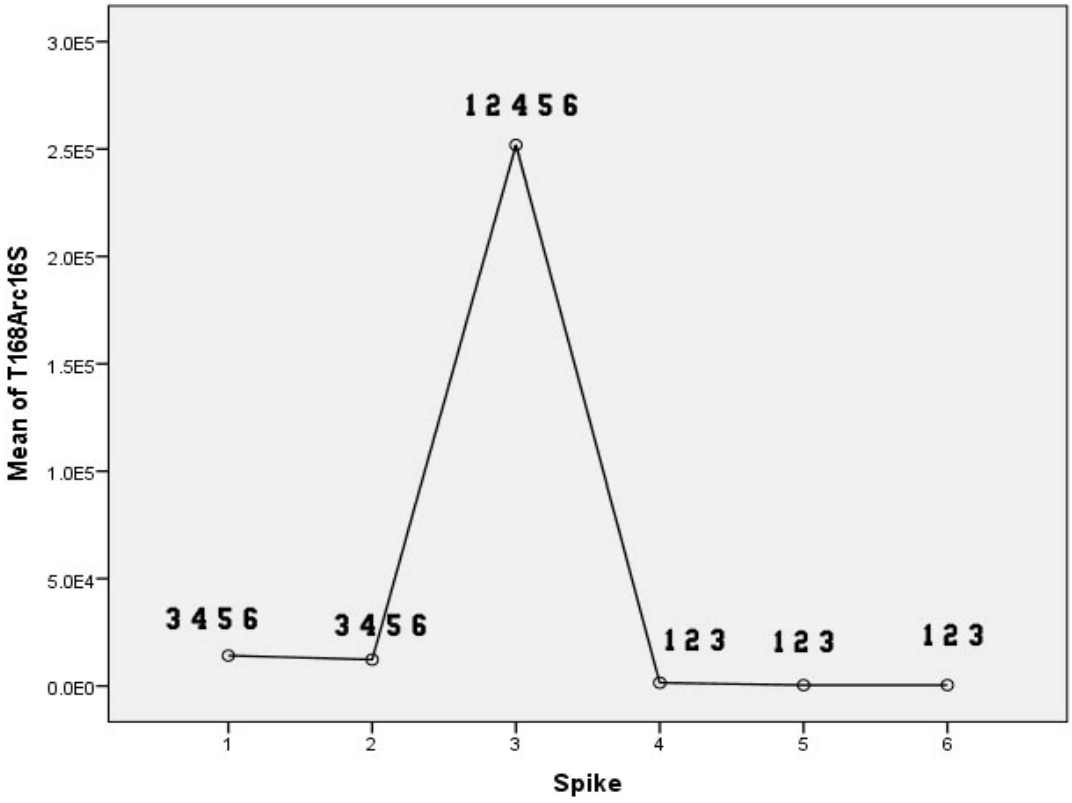
Mean of T168Arc16S
3.0E5
2.5E5
2.0E5
1.5E5
1.0E5
5.0E4
0.0E0
1 2 4 5 6
3 4 5 6
3 4 5 6
1 2 3
1 2 3
1 2 3
1
2
3
4
5
6
Spike

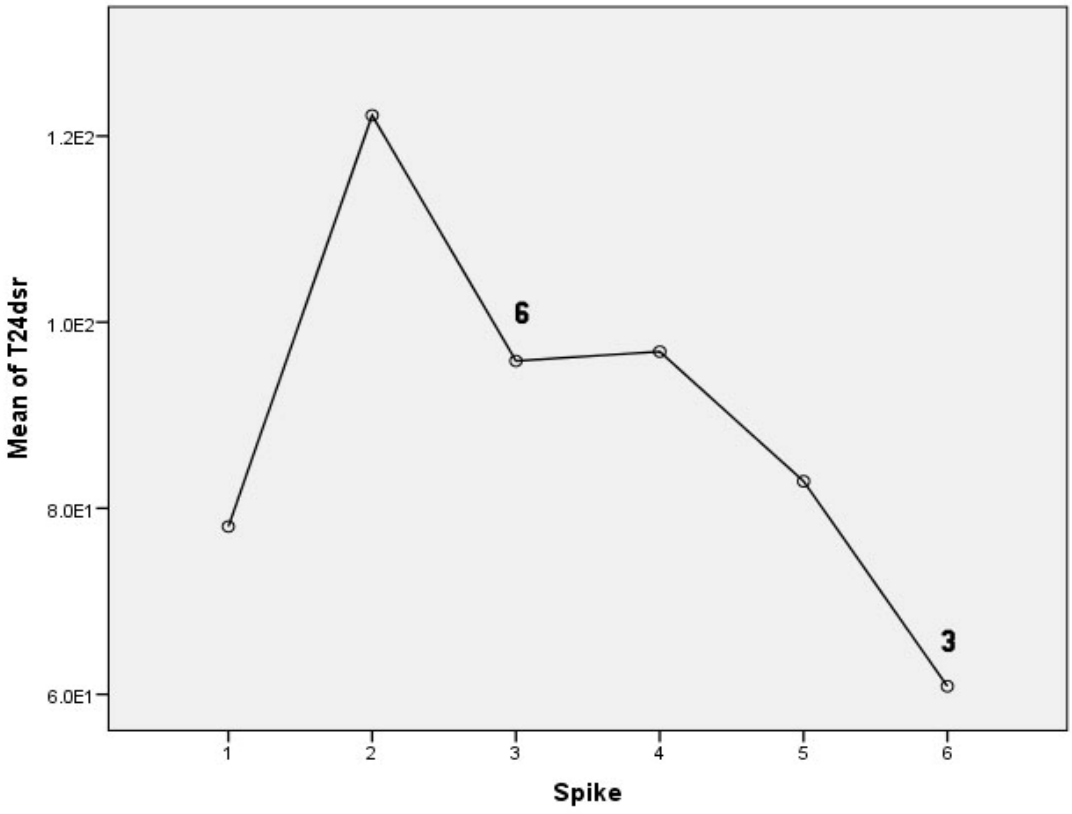
Mean of T24dsr
1.2E2
1.0E2
8.0E1
6.0E1
6
3
1
2
3
4
5
6
Spike

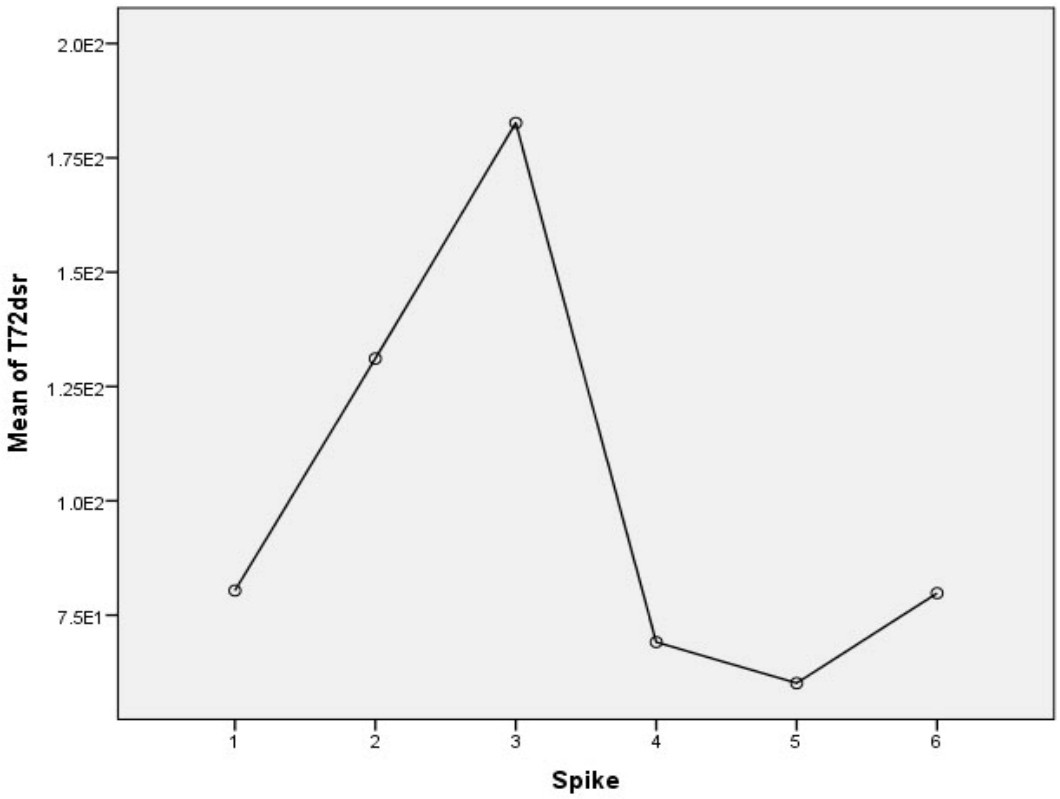
2.0E2
1.75E2
1.5E2
1.25E2
1.0E2
7.5E1
Mean of T72dsr
1
2
3
4
5
6
Spike

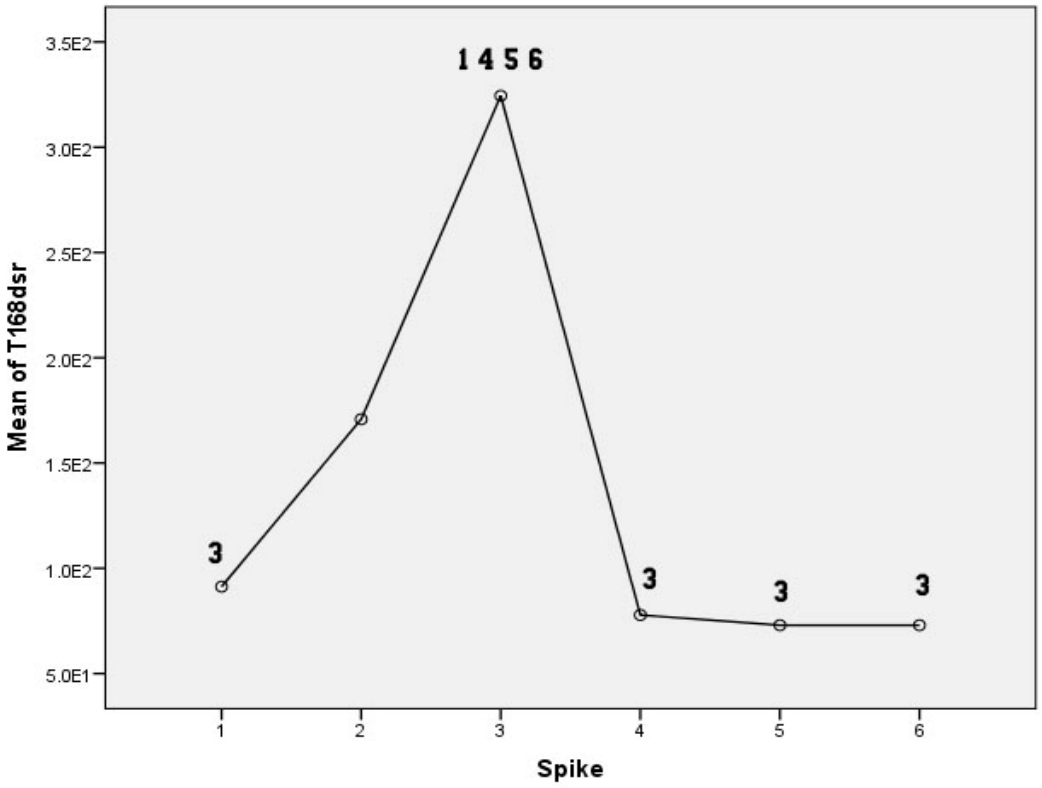
3.5E2
3.0E2
2.5E2
2.0E2
1.5E2
1.0E2
5.0E1
Mean of T168dsr
1 4 5 6
3
3
3
3
1
2
3
4
5
6
Spike

References

(1) Stroo, H. F.; Ward, C. H.: *In Situ Remediation of Chlorinated Solvent Plumes*; Springer: New York, 2010.

(2) *Natural Attenuation of Chlorinated Volatile Organic Compounds in a Freshwater Tidal Wetland;* U.S. Department of the Interior, U. S. G. S.: Aberdeen Proving Ground, MD, 1997.

(3) *Natural Attenuation of Chlorinated Volatile Organic Compounds in Ground Water at Operable Unit 1, Naval Undersea Warfare Center, Division Keyport, Washington;* U.S. Department of the Interior, U. S. G. S.: Tacoma, WA, 2002.

(4) Rivett, M. O.; Wealthall, G. P.; Dearden, R. A.; McAlary, T. A. Review of Unsaturated-Zone Transport and Attenuation of Volatile Organic Compound (VOC) Plumes Leached from Shallow Source Zones. *J. Contam. Hydrol.* **2011**, *123*, 130-156.

(5) Rathbun, R. E. Transport, Behavior, and Fate of Volatile Organic Compounds in Streams. *Environ. Sci. Technol.* **2000**, *30*, 129-295.

(6) Chapman, S. W.; Parker, B. L.; Cherry, J. A.; Aravena, R.; Hunkeler, D. Groundwater-Surface Water Interaction and its Role on TCE Groundwater Plume Attenuation. *J. Contam. Hydrol.* **2007**, *91*, 203-232.

(7) Gullickson, R. *Reference Data Sheet on Common Chlorinated Solvents.*

(8) *Toxicological Profile for Trichloroethylene;* U.S. Department of Health and Human Services, P. H. S., Agency for Toxic Substances and Disease Registry (ATSDR): Atlanta, GA, 1997.

(9) *TCE Removal from Contaminated Soil and Groundwater;* U.S. Environmental Protection Agency, O. o. R. a. D.: Ada, OK, 1992.

(10) Trichloroethylene. In *MSDS# 23850*; Fisher Scientific: Fair Lawn, NJ, 2008.

(11) *Trichloroethylene Health Risk Assessment: Synthesis and Characterization;* U.S. Environmental Protection Agency, N. C. f. E. A.: Washington, DC, 2001.

(12) Schwarzenbach, R. P.; Gschwend, P. M.; Imboden, D. M.: *Environmental Organic Chemistry, 2nd ed.*; John Wiley & Sons, Inc.: Hoboken, NJ, 2003.

(13) Harkness, M.; Fisher, A.; Lee, M. D.; Mack, E. E.; Payne, J. A.; Dworatzek, S.; Roberts, J.; Acheson, C.; Herrmann, R.; Possolo, A. Use of Statistical Tools to Evaluate the Reductive Dechlorination of High Levels of TCE in Microcosm Studies. *J. Contam. Hydrol.* **2012**, *131*, 100-118.

(14) Dolfing, J.: Hydrogen Cycling in Dechlorinating Ecosystems. In *ACS Symposia on Chemical-Biological Interactions in Contaminant Fate* 2000; Vol. 40; pp 328-330.

(15) Cis-1,2-Dichloroethylene. In *MSDS# 97773*; Acros Organic: Fair Lawn, NJ, 2009.

(16) Vinyl Chloride. In *MSDS# M9192*; OxyVinyls: Dallas, TX, 2009.

(17) Fantroussi, S. E.; Naveau, H.; Agathos, S. N. Anaerobic Dechlorinating Bacteria. *Biotechnol. Prog.* **1998**, *14*, 167-188.

(18) Loffler, F. E.; Cole, J. R.; Ritalahti, K. M.; Tiedhe, J. M.: Dehalogenation: Microbial Processes and Environmental Applications. Haggblom, M. M., Bossert, I. D., Ed.; Kluwer Academic Publishers: Norwell, MA, 2003; pp 53-87.

(19) Dennis, P. C.; Sleep, B. E.; Fulthorpe, R. R.; Liss, S. N. Phylogenetic Analysis of Bacterial Populations in an Anaerobic Microbial Consortium Capable of Degrading Saturation Concentrations of Tetrachloroethylene. *Can. J. Microbiol.* **2003**, *49*, 15-27.

(20) Sung, Y. Isolation and Ecology of Bacterial Populations Involved in Reductive Dechlorination of Chlorinated Solvents. Georgia Institute of Technology, 2005.

(21) Futagami, T.; Okamoto, F.; Hashimoto, H.; Fukuzawa, K.; Higashi, K.; Hazmul Hussain Nazir, K. H. M.; Wada, E.; Suyama, A.; Takegawa, K.; Goro, M.; Nakamura, K.; Furukawa, K. Enrichment and Characterization of a Trichloroethene-Dechlorinating Consortium Containing Multiple “Dehalococcoides” Strains. *Biosci. Biotechnol. Biochem.* **2011**, *75*, 1268-1274.

(22) Witt, M. E.; Klecka, G. M.; Lutz, E. J.; Ei, T. A.; Grosso, N. R.; Chapelle, F. H. Natural Attenuation of Chlorinated Solvents at Area 6, Dover Air Force Base: Groundwater Biogeochemistry. *J. Contam. Hydrol.* **2002**, *57*, 61-80.

(23) Muller, N. C.; Nowack, B.: Nano Zero Valent Iron – The Solution for Water and Soil Remediation? In *ObservartoryNANO*, 2010; pp 1-34.

(24) Higgins, M. R.; Olson, T. M. Life-Cycle Case Study Comparison of Permeable Reactive Barrier versus Pump-and-Treat Remediation. *Environ. Sci. Technol.* **2009**, *43*, 9432-9438.

(25) Henderson, A. D.; Demond, A. H. Long-Term Performance of Zero-Valent Iron Permeable Reactive Barriers: A Critical Review. *Environ. Eng. Sci.* **2007**, *24*, 401-423.

(26) *Zero-Valent Iron Reactive Materials for Hazardous Waste and Inorganics Removal*; American Society of Civil Engineers: Virginia, 2007.

(27) Permeable Reactive Barriers & Reactive Zones. In *Vision on Technology*; Bastiaens, L., Ed.: Belgium, 2010.

(28) Weber, E. J. Iron-Mediated Reductive Transformations: Investigation of Reaction Mechanism. *Environ. Sci. Technol.* **1996**, *30*, 716-719.

(29) Song, H.; Carraway, E. R. Reduction of Chlorinated Ethanes by Nanosized Zero-Valent Iron: Kinetics, Pathways, and Effects of Reaction Conditions. *Environ. Sci. Technol.* **2005**, *39*, 6237-6245.

(30) Zhang, Z.; Hao, Z.; Yang, Y.; Zhang, J.; Wang, Q.; Xu, X. Reductive Denitrification Kinetics of Nitrite by Zero-Valent Iron. *Desalination* **2010**, *252*, 158-162.

(31) Grieger, K. D.; Fjordboge, A.; Hartmann, N. B.; Eriksson, E. Environmental Benefits and Risks of Zero-Valent Iron Nanoparticles (nZVI) for in situ Remediation: Risk Mitigation or Trade-Off? *J. Contam. Hydrol.* **2010**, *118*, 165-183.

(32) Kanel, S. R.; Greneche, J.-M.; Choi, H. Arsenic(V) Removal from Groundwater Using Nano Scale Zero-Valent Iron as a Colloidal Reactive Barrier Material. *Environ. Sci. Technol.* **2006**, *40*, 2045-2050.

(33) Hwang, Y.-H.; Kim, D.-G.; Shin, H.-S. Mechanism Study of Nitrate Reduction by Nano Zero Valent Iron. *J. Hazard. Mater.* **2011**, *185*, 1513-1521.

(34) Ramos, M. A. V.; Yan, W.; Li, X.-Q.; Koel, B. E.; Zhang, W.-X. Simultaneous Oxidation and Reduction of Arsenic by Zero-Valent Iron Nanoparticles: Understanding the Significance of the Core-Shell Structure. *J. Phys. Chem. C.* **2009**, *113*, 14591-14594.

(35) Reinsch, B. C.; Forsberg, B.; Penn, R. L.; Kim, C. S.; Lowry, G. V. Chemical Transformations during Aging of Zerovalent Iron Nanoparticles in the Presence of Common Groundwater Dissolved Constituents. *Environ. Sci. Technol.* **2010**, *44*, 3455-3461.

(36) Li, X.-Q.; Elliot, D. E.; Zhang, W.-X. Zero-Valent Iron Nanoparticles for Abatement of Environmental Pollutants: Materials and Engineering Aspects. *Crit. Rev. Solid State Mater. Sci.* **2006**, *31*, 111-122.

(37) Cirtiu, C. M.; Raychoudhury, T.; Ghoshal, S.; Moores, A. Systematic Comparison of the Size, Surface Characteristics, and Colloidal Stability of Zero Valent Iron Nanoparticles Pre- and Post- Grafted with Common Polymers. *Colloids Surf., A.* **2011**, *390*, 95-104.

(38) Goldstein, N.; Greenlee, L. F. Influence of Synthesis Parameters on Iron Nanoparticle Size and Zeta Potential. *J. Nanopart. Res.* **2012**, *14*.

(39) Sun, Y.-P.; Li, X.-Q.; Zhang, W.-X.; Wang, H. P. A Method for the Preparation of Stable Dispersion of Zero-Valent Iron Nanoparticles. *Colloids Surf., A.* **2007**, *308*, 60-66.

(40) Wiesner, M. R.; Lowry, G. V.; Jones, K. L.; Hochella, M. F.; Di Giulio, R. T.; Casman, E.; S., B. E. Decreasing Uncertainties in Assessing Environmental Exposure, Risk, and Ecological Implications of Nanomaterials. *Environ. Sci. Technol.* **2009**, *43*, 6458-6462.

(41) Neal, A. L. What can be Inferred from Bacterium-Nanoparticle Interactions about the Potential Consequences of Environmental Exposure to Nanoparticles? *Ecotoxicology* **2008**, *17*, 362-371.

(42) Dreher, K. L. Health and Environmental Impact of Nanotechnology: Toxicological Assessment of Manufactured Nanoparticles. *Toxicol. Sci.* **2004**, *77*, 3-5.

(43) Lanone, S.; Rogerieux, F.; Geys, J.; Dupont, A.; Maillot-Marechal, E.; Boczkowski, J. l.; Lacroix, G.; Hoet, P. Comparative Toxicity of 24 Manufactured Nanoparticles in Human Alveolar epithelial and Macrophage Cell Lines. *Part. Fibre Toxicol.* **2009**, *6*.

(44) Nel, A.; Xia, T.; Madler, L.; Li, N. Toxic Potential of Materials at the Nanolevel. *Science* **2006**, *311*, 622-627.

(45) Carlson, C.; Hussain, S. M.; Schrand, A. M.; Braydich-Stolle, L. K.; Hess, K. L.; Jones, R. L.; Schlager, J. J. Unique Cellular Interaction of Silver Nanoparticles: Size-Dependent Generation of Reactive Oxygen Species. *J. Phys. Chem. B.* **2008**, *112*, 13608-13619.

(46) Sager, T. M.; Castranova, V. Surface Area of Particle Administered versus Mass in Determining the Pulmonary Toxicity of Ultrafine and Fine Carbon Black: Comparison to Ultrafine Titanium Dioxide. *Part. Fibre Toxicol.* **2009**, *6*.

(47) Diao, M.; Yao, M. Use of Zero-Valent Iron Nanoparticles in Inactivating Microbes. *Water Res.* **2009**, *43*, 5243-5251.

(48) Lee, C.; Kim, J. Y.; Lee, W. I.; Nelson, K. L.; Yoon, J.; Sedlak, D. L. Bactericidal Effect of Zero-Valent Iron Nanoparticles on Escherichia coli. *Environ. Sci. Technol.* **2008**, *42*, 4927-4933.

(49) Xiu, Z.-M.; Gregory, K. B.; Lowry, G. V.; Alvarez, P. J. J. Effect of Bare and Coated Nanoscale Zerovalent Iron on tceA and vcrA Gene Expression in Dehalococcoides spp. *Environ. Sci. Technol.* **2010**, *44*, 7647-7651.

(50) Fajardo, C.; Ortiz, L. T.; Rodriguez-Membibre, M. L.; Nande, M.; Lobo, M. C.; Martin, M. Assessing the Impact of Zero-Valent Iron (ZVI) Nanotechnology on Soil Microbial Structure and Functionality: A Molecular Approach. *Chemosphere* **2012**, *86*, 802-808.

(51) Barnes, R. J.; Van der Gast, C. J.; Riba, O.; Lehtovirta, L. E.; Prosser, J. I.; Dobson, P. J.; Thompson, I. P. The Impact of Zero-Valent Iron Nanoparticles on a River Water Bacterial Community. *J. Hazard. Mater.* **2010**, *184*, 73-80.

(52) Li, Z.; Greden, K.; Alvarez, P. J. J.; Gregory, K. B.; Lowry, G. V. Adsorbed Polymer and NOM Limits Adhesion and Toxicity of Nano Scale Zerovalent Iron to E. coli. *Environ. Sci. Technol.* **2010**, *44*, 3462-3467.

(53) Zhang, W.-X. Nanoscale Iron Particles for Environmental Remediation: An Overview. *J. Nanopart. Res.* **2003**, *5*, 323-332.

(54) Crane, R. A.; Scott, T. B. Nanoscale Zero-Valent Iron: Future Prospects for an Emerging Water Treatment Technology. *J. Hazard. Mater.* **2012**, *211*, 112-125.

(55) BMT Entech, I. *Remedial Investigation Report for the Beaverdam Road Landfill*: Beltsville, MD2008.

(56) RNeasy Mini Handbook. 4th ed.; Qiagen, 2010.

(57) Power SYBR Green PCR Master Mix and Power SYBR Green RT-PCR Reagents Kit User Guide. Life Technologies: Carlsbad, CA, 2011.

(58) TaqMan Fast Advanced Master Mix Protocol. Life Technologies: Carlsbad, CA, 2011.

(59) Fierer, N.; Jackson, J. A.; Vilgalys, R.; Jackson, R. B. Assessment of Soil Microbial Community Structure by Use of Taxon-Specific Quantitative PCR Assays. *Appl. Environ. Microbiol.* **2005**, *71*, 4117-4120.

(60) Yarwood, S. A.; Bottomley, P. J.; Myrold, D. D. Soil Microbial Communities Associated with Douglas-fir and Red Alder Stands at High- and Low-Productivity Forest Sites in Oregon, USA. *Microb. Ecol.* **2010**, *60*, 606-617.

(61) Wilms, R.; Sass, H.; Kopke, B.; Cypionka, H.; Engelen, B. Methane and Sulfate Profiles within the Subsurface of a Tidal Flat are Reflected by the Distribution of Sulfate-Reducing Bacteria and Methanogenic Archaea. *FEMS Microbiol. Ecol.* **2007**, *59*, 611-621.

(62) Lever, M. A. Anaerobic Carbon Cycling Pathways in the Subseafloor Investigated via Functional Genes, Chemical Gradients, Stable Carbon Isotopes, and Thermodynamic Calculations. University of North Carolina at Chapel Hill, 2008.

(63) Eilert, K. D.; Foran, D. R. Polymerase Resistance to Polymerase Chain Reaction Inhibitors in Bone. *J. Forensic Sci.* **2009**, *54*, 1001-1007.

(64) Teng, F.; Guan, Y.; Zhu, W. A Simple and Effective Method to Overcome the Inhibition of Fe to PCR. *J. Microbiol. Meth.* **2008**, *75*, 362-364.

(65) van Pelt-Verkuil, E.; van Belkum, A.; Hays, J. P.: *Principles and Technical Aspects of PCR Amplification*; Springer: Netherlands, 2008. pp. 39-44.

(66) Kreader, C. A. Relief of Amplification Inhibition in PCR with Bovine Serum Albumin or T4 gene 32 Protein. *Appl. Environ. Microbiol.* **1996**, *62*, 1102-1106.

(67) GenEx 5 Efficiency Correction. http://www.multid.se/genex/hs130.htm (accessed 05/23/13 2013).

(68) One-way ANOVA in SPSS. https://statistics.laerd.com/spss-tutorials/one-way-anova-using-spss-statistics.php.

(69) Zetasizer Nano User Manual. Malvern Instruments Ltd.: Worcestershire, UK, 2007.

(70) Sun, Y.-P.; Li, X.-Q.; Cao, J.; Zhang, W.-X.; Wang, P. H. Characterization of Zero-Valent Iron Nanoparticles. *Adv. Colloid Interface Sci.* **2006**, *120*, 47-56.

(71) Nurmi, J. T.; Tratnyek, P. G.; Sarathy, V.; Baer, D. R.; Amonette, J. E.; Pecher, K.; Wang, C.; Linehan, J. C.; Matson, D. W.; Penn, R. L.; Driessen, M. D. Characterization and Properties of Metallic Iron Nanoparticles: Spectroscopy, Electrochemistry, and Kinetics. *Environ. Sci. Technol.* **2005**, *39*, 1221-1230.

(72) Zhang, Z.; Zhang, X.; Xin, Z.; Deng, M.; Wen, Y.; Song, Y. Synthesis of Monodisperse Silver Nanoparticles for Ink-Jet Printed Flexible Electronics. *Nanotechnology* **2011**, *22*, 1-8.

(73) Kang, S. E.; Kang, Y. S. Silver Nanoparticles Stabilized by Crosslinked Poly(Vinyl Pyrrolidone) and its Application for Facilitated Olefin Transport. *J. Colloid and Interface Sci.* **2011**, *353*, 83-86.

(74) Handbook of Environmental Site Characterization and Ground-Water Monitoring. 2nd ed.; Nielsen, D. M., Ed.; Taylor & Francis Group: Boca Raton, FL, 2006; pp 616-627.

(75) Gaal, R.; Barlett, M. S.; Ross, W.; Turnbough, C. L.; Gourse, R. L. Transcription Regulation by Initiating NTP Concentration: rRNA Synthesis in Bacteria. *Science* **1997**, *278*, 2092-2097.

(76) Kemp, P. F.; Lee, S.; LaRoche, J. Estimating the Growth Rate of Slowly Growing Marine Bacteria from RNA Content. *Appl. Environ. Microbiol.* **1993**, *59*, 2594-2601.

(77) Klindworth, A.; Pruesse, E.; Schweer, T.; Pepliers, J.; Quast, C.; Horn, M.; Glockner, F. O. Evaluation of General 16S Ribosomal RNA Gene PCR Primers for Classical and Next-Generation Sequencing-Based Diversity Studies. *Nucl. Acids Res.* **2012**.

(78) Horz, H. P.; Vianna, M. E.; Gomes, B. P. F. A.; Conrads, G. Evaluation of Universal Probes and Primer Sets for Assessing Total Bacterial Load in Clinical Samples: General Implications and Practical Use in Endodontic Antimicrobial Therapy *J. Clin. Microbiol.* **2005**, *43*, 5332-5337.

(79) Crespo, J.; Garcia-Barrasa, J.; Lopez-de-Luzuriaga, J. M.; Monge, M.; Olmos, E. M.; Saenz, Y.; Torres, C. Organometallic Approach to Polymer-Protected Antibacterial Silver Nanoparticles: Optimal Nanoparticle Size-Selection for Bacteria Interaction. *J. Nanopart. Res.* **2012**, *14*, 1-13.

(80) Huang, Y. H.; Zhang, T. C. Effects of Dissolved Oxygen on Formation of Corrosion Products and Concomitant Oxygen and Nitrate Reduction in Zero-Valent Iron Systems with or without Aqueous Fe2+. *Water Res.* **2005**, *39*, 1751-1760.

(81) O'Flaherty, V.; Mahony, T.; O'Kennedy, R.; Colleran, E. Effect of pH on Growth Kinetics and Sulphide Toxicity Thresholds of a Range of Methanogenic, Syntrophic and Sulphate-Reducing Bacteria. *Process Biochem.* **1998**, *33*, 555-569.

(82) Lowe, S. E.; Jain, M. K.; Zeikus, G. Biology, Ecology, and Biotechnological Applications of Anaerobic Bacteria Adapted to Environmental Stresses in Temperature, pH, Salinity, or Substrates. *Microbio. Reviews* **1993**, *57*, 451-509.

(83) Watt, B.; Brown, F. V. Effect of the Growth of Anaerobic Bacteria on the Surface pH of Solid Media. *J. Clin. Pathol.* **1985**, *38*, 565-569.

(84) Vasilian, A.; Trchunian, A. Effect of the Medium Redox Potential on the Growth and Metabolism of Anaerobic Bacteria. *Biofizika* **2008**, *53*, 281-293.

(85) Wang, Z. P.; DeLaune, R. D.; Patrick, W. H.; Masscheleyn, P. H. Soil Redox and pH Effects on Methane Production in a Flooded Rice Soil. *Soil Sci. Soc. of America* **1993**, *57*, 382-385.

(86) Hunting, E. R.; Kampfraath, A. A. Contribution of Bacteria to Redox Potential (E h) Measurements in Sediments. *Int. J. Environ. Sci. Technol.* **2013**, *10*, 55-62.

(87) Baker, C.; Pradhan, A.; Pakstis, L.; Darrin, P. J.; Ismat, S. S. Synthesis and Antibacterial Properties of Silver Nanoparticles. *J. Nanosci. Nanotechno.* **2005**, *5*, 244-249.

(88) Shrivastava, S.; Bera, T.; Roy, A.; Singh, G.; Ramachandrarao, P.; Dash, D. Characterization of Enhanced Antibacterial Effects of Novel Silver Nanoparticles. *Nanotechnology* **2007**, *18*.

(89) Kim, S. J.; Kuk, E.; Yu, K. N.; Kim, J.-H.; Park, S. J.; Lee, H. J.; Kim, S. H.; Park, Y. K.; Park, Y. H.; Hwang, C.-Y.; Kim, Y.-K.; Lee, Y.-L.; Jeong, H.; Cho, M.-H. Antimicrobial Effects of Silver Nanoparticles. *Nanomed.-Nanotechnol.* **2007**, *3*, 95-101.

(90) Lu, Z.; Rong, K.; Li, J.; Yang, H.; Chen, R. Size-Dependent Antibacterial Activities of Silver Nanoparticles Against Oral Anaerobic Pathogenic Bacteria. *J. Mater. Sci. - Mater. Med.* **2013**, *24*, 1465-1471.

(91) Lara, H. H.; Ayala-Nunez, N. V.; del Carmen Ixtepan Turrent, L.; Padilla, C. R. Bactericidal Effect of Silver Nanoparticles against Multidrug-Resistant Bacteria. *World J. Microb. Biot.* **2010**, *26*, 615-621.

(92) Du, H.; Lo, T.-M.; Sitompul, J.; Chang, M. W. Systems-Level Analysis of Escherichia coli Response to Silver Nanoparticles: The Roles of Anaerobic Respiration in Microbial Resistance. *Biochem. Biophys. Res. Comm.* **2012**, *424*, 657-662.

(93) Doolette, C. L.; McLaughlin, M. J.; Kirby, J. K.; Batstone, D. J.; Harris, H. H.; Ge, H.; Cornelis, G. Transformation of PVP Coated Silver Nanoparticles in a Simulated Wastewater Treatment Process and the Effect on Microbial Communities. *Chem. Cent. J.* **2013**, *7*.

(94) Xiu, Z.-M.; Zhang, Q.-B.; Puppala, H. L.; Colvin, V. L.; Alvarez, P. J. J. Negligible Particle-Specific Antibacterial Activity of Silver Nanoparticles. *Nano Letters* **2012**, *12*, 4271-4275.

(95) Yang, Y.; Chen, Q.; Wall, J. D.; Hu, Z. Potential Nanosilver Impact on Anaerobic Digestion at Moderate Silver Concentrations. *Water Res.* **2012**, *46*, 1176-1184.